CENTER FOR ASTROPHYSICS
HARVARD & SMITHSONIAN

Submillimeter Array Newsletter

Number 30, July 2020

CONTENTS

1 From the Director

SCIENCE HIGHLIGHTS:

2 A Three Dimensional View of Gomez's Hamburger

5 Physical Conditions and Kinematics of the Filamentary Structure in Orion Molecular Cloud 1

8 CMZoom: Survey Overview and First Data Release

14 Beyond Our Local Horizon: Dust Continuum Observations of Individual Giant Molecular Clouds Across Andromeda's Neighborhoods

TECHNICAL HIGHLIGHTS:

18 The Quest to Design the wSMA Vacuum Window

21 RTDC Update

OTHER NEWS

22 Receiver Lab Talks

Call For Standard Observing Proposals

23 Postdoctoral Opportunities with the SMA

24 SMA Postdoctoral Fellows: Comings and Goings

25 Staff Changes in Hilo

Proposal Statistics

26 Track Allocations

Top-Ranked SAO and ASIAA Proposals

27 All SAO Proposals

28 Recent Publications

FROM THE DIRECTOR

Dear SMA Newsletter readers,

During these challenging times, we are fortunate that most of us are able to efficiently accomplish our engineering and scientific work through teleworking at home. As we do so, we remain mindful of, and grateful for, the work of those in our communities who cannot do this, and whose work supports all of us.

Observatory operations do require staff members at the SMA site in order to ensure safe and efficient operation of the SMA, be it for on-sky testing of ongoing upgrades, system calibration, or astronomical observations. In response to the pandemic, the SMA shut down observing programs in mid-March. However, as Hawaii has thus far been less hard-hit by the pandemic than much of the world, we were able to resume nightly observing following an 11-week hiatus. The SMA is currently operating on a reduced schedule, however many science observations have been made since we decided to return to the skies. I am indebted to all our SMA Hawaii-based staff for their unselfish efforts in making this possible, and to other SMA staff members based in Cambridge and Taipei for providing assistance and guidance as needed.

Many other observatories, including ALMA and the ACA, face more challenging circumstances and have not yet been able to resume operations. We invite members of our community, particularly those needing time-sensitive observations of variable or transient phenomena, or other time-critical data in support of a project or proposal, to contact SMA_DDT@cfa.harvard.edu if you believe the SMA may be able to help during this period. Despite our reduced schedule, we may be able to find you time.

We expect that we will not return to full-scale scientific operations for some time yet, and so have decided to increase the percentage of time made available to small programs - those that require just a few hours of on-sky time to enable a scientifically-worthy result, or to enable larger, more significant observing programs to be proposed to the SMA or other observatories in the future. Please take a look at the SMA call for observing proposals, which will be announced early August, for more details. In the interim, stay safe.

Best wishes,

Raymond Blundell

A THREE DIMENSIONAL VIEW OF GOMEZ'S HAMBURGER

Richard Teague (CfA), Marija R. Jankovic (Imperial College London), Thomas J. Haworth (Queen Mary University), Chunhua Qi (CfA), John D. Ilee (University of Leeds)

Characterising the three dimensional physical and chemical structure of a protoplanetary disk, the birthplace of planets, is an essential step in understanding the formation and subsequent evolution of young planets. Of particular importance is how the gas mass is distributed throughout the disk, and the local temperature, two variables that set the pace and efficiency of planet formation.

In this work we apply new analysis techniques to archival SMA data of 'Gomez's Hamburger' (GoHam; 2MASS J16281370-2431391), a massive, nearly edge-on disk. The name comes from the unique morphology of the emission seen at shorter wavelengths with the Hubble Space Telescope: a dark, elongated lane bounded by two bright arcs of light . This structure naturally arises for edge-on disks as large dust grains settle towards the midplane and block the light from the central star. It is only through the tops of the disk that light can escape. Smaller dust grains are able to scatter the light from the star and towards us, over the top of the disk. At submillimeter wavelengths the extended gas structure and concentrated grains are clearly visible, as shown in Fig. 1.

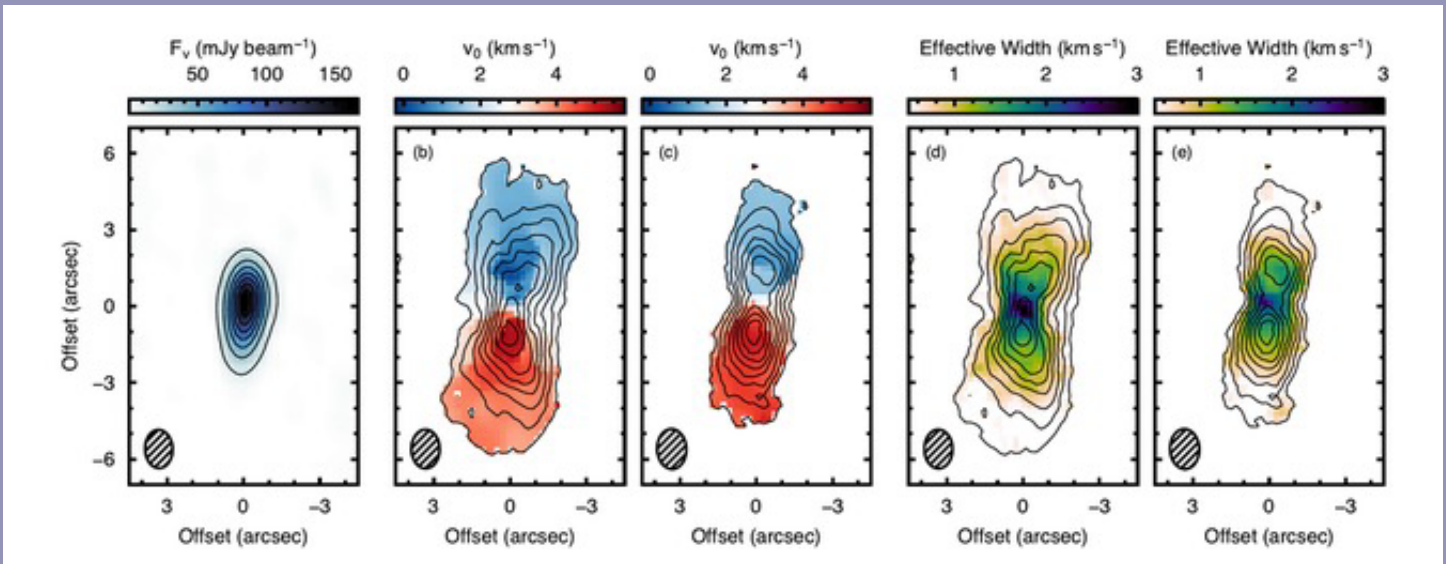

Figure 1: Compendium of SMA observations of GoHam. The left panel shows the 1.3mm continuum, tracing large dust particles which have settled to the disk midplane. The central two panels show the ^{12}CO (2 - 1) and ^{13}CO (2 - 1) emission and their projected line-of-sight velocity, considerably more extended than the continuum. The final two panels show the effective width of the two emission lines.

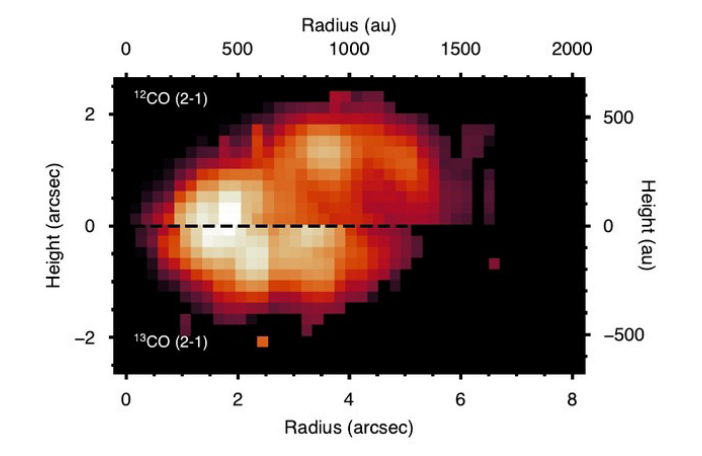

Figure 2: Comparison of the ^{12}CO (2 - 1) and ^{13}CO (2 - 1) emission layers, top and bottom, respectively using the 'tomographically reconstructed distribution'. The ^{12}CO emission can be clearly seen to arise from a more elevated region than the ^{13}CO and extending out to larger radii.

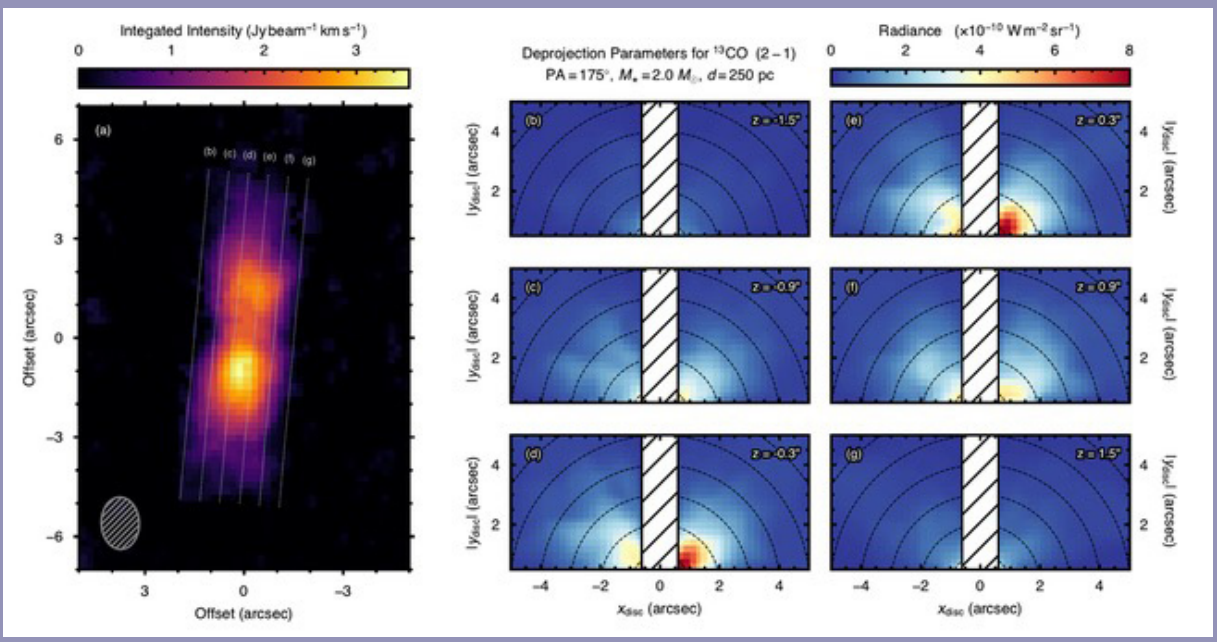

Figure 3: The integrated intensity map of ^{13}CO (2 - 1), left. The dotted lines show cuts in the emission at distinct heights in the disk, relating to the panels on the right. Each of these panels show a face-down view of the disk (counter to the edge-on view of the left panel). In each of these panels, the x-axis represents the dotted lines in the left panel, while the y axis represents along the line of fight. In each panel the ^{13}CO emission can be seen to drop off radially, as expected, but also the hint of an excess in emission close to the midplane (z = 0), and to positive x-values. We interpret this excess emission as GoHam b.

While the edge-on view of the disk allows for stunning images at shorter wavelengths, it has long proved a challenge to understand the distribution of the gas along the line-of-sight. Original work presented in Bujarrabal et al. (2008, 2009) showed that the authors were able to fit an azimuthally symmetric disk model to observations of ^{12}CO, ^{13}CO and C^{18}O emission, detecting the presence of an enhancement in emission in the southern side of the disk. More recent observations of the 8.6μm and 11.2μm PAH emission using ESO's Very Large Telescope, Berné et al. (2015), confirm that an overdensity at this location is present and could potentially be a still-forming planet, GoHam b.

To explore this scenario, we have applied the techniques described in Dent et al. (2014) and Dutrey et al. (2017) which relates the projected line-of-sight velocity (central panels in Fig. 1) to the line-of-sight distance, assuming that the disk is in Keplerian rotation. This provides a unique opportunity

to translate the three dimensional position-position-velocity data obtained from the SMA to a full three dimensional position-position-position cube. In this work we were able to extend these methods to account for deviations in the disk rotation profile expected for geometrically thick disks.

To explore the vertical structure of the disk we calculate the 'tomographic reconstructed distribution', coined by Dutrey et al. (2017), shown in Fig. 2. This compares the emission heights of two molecules, ^{12}CO, top, and ^{13}CO, bottom, revealing two distinct emission distributions, namely that ^{12}CO traces highly elevated and radially extended regions, while the ^{13}CO, due to its lower abundance, tracers far closer to the disk midplane and is not as radially extended. These results demonstrate the utility in such observations in mapping out the chemical structure of these planet forming disks. Coupled with the large bandwidth and high spectral resolution of the current SMA, new observations would allow us to map the vertical and radial distribution of a range of molecular species, a task as of yet unable to be achieved with less significantly inclined disks.

In addition to the vertical distribution of molecules, the techniques outlined in Dent et al. (2014) allow us to deproject the data into face-on projections, as shown in Fig. 3. Here we show how the edge-on data can be deprojected into top-down views of the disk for given slices. What is most intriguing about these deprojections is that we now have access to line-of-sight information. In particular, we are able to localize the enhanced emission in the southern side of the disk previously reported and interpreted as GoHam b. Although limited by the spatial resolution of the archival data, these results demonstrate a hugely exciting approach to characterising GoHam b. Newer observations with the SMA achieving higher spatial and spectral resolutions will enable us to fully characterise GoHam b and its local environment in 3D, allowing for one of the most thorough characterizations of the planet formation process to date.

In conclusion, these results demonstrate the potential of edge-on sources in characterising both the planet formation and the evolution of the planet-hosting disk. The SMA is uniquely poised with its large bandwidth to undertake spectral surveys, mapping out the chemical structure in three dimensions. Coupled with contemporary simulations of planet-disk interactions, these observed chemical and physical structures will open up an entirely new perspective of protoplanetary disks.

REFERENCES

- Berné O., et al., 2015, A&A, 578, L8
- Bujarrabal V., Young K., Fong D., 2008, A&A, 483, 839
- Bujarrabal V., Young K., Castro-Carrizo A., 2009, A&A, 500, 1077
- Dent W. R. F., et al., 2014, Science, 343, 1490
- Dutrey A., et al., 2017, A&A, 607, A130

PHYSICAL CONDITIONS AND KINEMATICS OF THE FILAMENTARY STRUCTURE IN ORION MOLECULAR CLOUD 1

Yu-Hsuan Teng (UCSD) and Naomi Hirano (ASIAA)

It is known that filamentary structures are prevalent in star-forming clouds and are believed to play an important role in star formation processes (e.g. Schneider & Elmegreen 1979; Andre et al. 2014). The sizes of filaments in star-forming regions range from parsec to subparsec scales, and a large-scale filament may consist of narrower filaments at a smaller scale. For example, the northern part of the Orion A molecular cloud, which is the nearest high-mass star-forming region at a distance of 414 pc (Menten et al. 2007), is an integral-shape filament with >13 pc long and ~0.5 pc wide (Bally et al. 1987). Residing at the center of the integral-shape filament, the Orion Molecular Cloud1 (OMC1) is the most massive component (>2200 $M_{\odot}$) and the most active star-forming region in the cloud (Bally et al. 1987). Previous interferometric observations of NH_3 with the Very Large Array (VLA) (Wiseman & Ho, 1998) and N_2H^+ 1–0 with the Atacama Large Millimeter/submillimeter Array (ALMA) (Hacar et al. 2018) revealed that OMC1 consists of smaller-scale filaments of high density gas. The dense cores inside these small-scale filaments could be current or future sites for star formation.

Using the Submillimeter Array (SMA), we have observed the N_2H^+ 3–2 emission from OMC1 at an angular resolution of ~5.4'' (~2300 au). Our 144-pointing mosaic observations covering the 6' × 9' (0.7 pc × 1.1 pc) area of OMC1 were combined with the single-dish data obtained with the Submillimeter Telescope (SMT) in order to recover the spatially extended emission. Figure 1 shows the combined moment 0 (integrated intensity) and moment 1 (intensity-weighted radial velocity) maps. The moment 0 map clearly shows that most of the

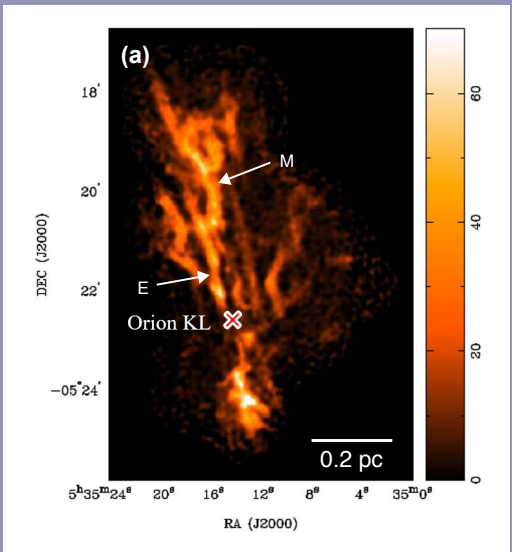

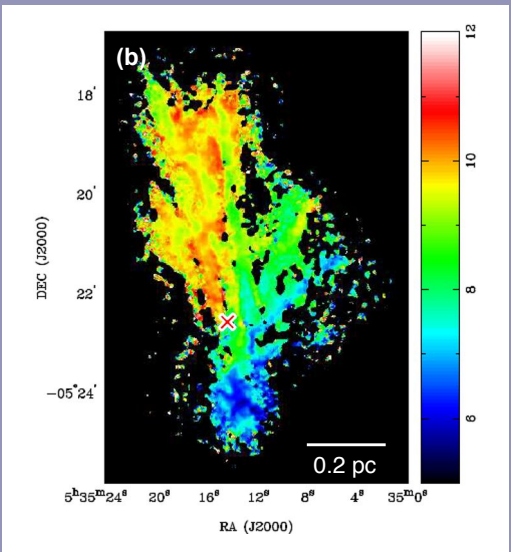

Figure 1a (left) **and 1b** (right): Moment 0 (K km s^{-1}) and moment 1 (km s^{-1}) maps of the combined SMA and SMT data in N_2H^+ 3–2. The cross depicts the position of Orion KL at (R.A., decl.) = (5^h 35^m $14^s.5$, -5°22'30''). The arrows indicate the two prominent filaments with core fragmentation.

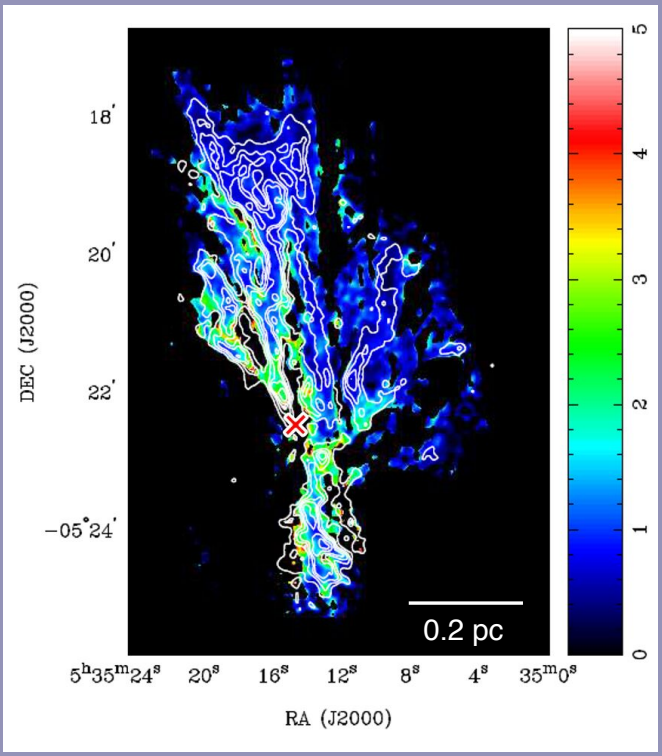

Figure 2: N_2H^+ 3–2/1–0 intensity ratio map using 1–0 image observed with ALMA + IRAM 30m (Hacar et al. 2018). Contour levels of N_2H^+ 3–2 moment 0 are overlaid on the line ratio map. The cross marks the position of Orion KL.

emission comes from the filamentary structure with a typical width of 0.02–0.03 pc. Several high-intensity and clumpy structures can also be seen inside the filaments. By applying *FilFinder* (Kock & Rosolowsky, 2015) and *2D Clumpfind* (Williams et al. 1994) on the combined image, we identified 11 filaments and 10 cores, respectively.

As revealed in Figure 1b, the OMC1 region consists of three subregions having different radial velocities with sharp velocity transitions. The northern region, with bright filaments to the north of Orion KL, has a velocity range of ~9–11 km s^{-1}; the western region, with fainter filaments extending to the northwest, is observed at ~7–9 km s^{-1}; and the southern region, also known as OMC1-South, is at ~5–7 km s^{-1}. These three subregions with different velocities converge at the Orion KL region. Such velocity structure of OMC1 can be interpreted as large-scale inflowing gas being accelerated toward the Orion Nebula Cluster (Peretto et al. 2013; Hacar et al. 2017). The morphology of magnetic fields in OMC1 observed by the JCMT BISTRO Survey (Pattle et al. 2017) also supports this global collapse scenario.

To analyze the physical conditions of the dense gas, we made the 3–2/1–0 ratio map (Figure 2) using our SMA + SMT data and the ALMA + IRAM 30 m data provided by Hacar et al. (2018). Using the non-LTE radiative transfer code RADEX (van der Tak et al. 2007), we modeled the integrated intensities of N_2H^+ 3–2 and 1–0 and the 3–2/1–0 intensity ratios under various combinations of H_2 density (n_{H2}), kinetic temperature (T_{kin}), and the ratio of N_2H^+ column density to line width ($N(N_2H^+)/\Delta v$).

The N_2H^+ 3–2/1–0 ratio map presented in Figure 2 reveals higher ratios overall in the eastern part of OMC1. In addition, the 3–2/1–0 ratio tends to be lower in the filament regions (1 ± 0.3) as compared to the surrounding nonfilament regions (2.2 ± 0.4). The non-LTE models have revealed that the filament regions have a higher density of ~10^7 cm^{-3} and a lower temperature of ~15–20 K than the nonfilament regions. Inside the filaments, the volume density of the core regions (1–3 × 10^7 cm^{-3}) are generally higher than the lower intensity regions (3–10 × 10^6 cm^{-3}), while there is no significant difference in temperature between the core and the lower intensity regions. Using the volume densities determined from the non-LTE analysis, we have estimated the masses of the cores and the line masses of the filaments. The masses of the cores are in the range of 1–10 $M_\odot$, which are similar to their virial masses. We also found that 7 of the 11 identified filaments have line masses between 0.5 to 1.5 times their critical line masses. These results indicate that most of the OMC1 filaments and cores are gravitationally bound.

The higher 3–2/1–0 ratio in the eastern part of OMC1 suggests that the eastern OMC1 has higher temperatures compared with the remaining area. The overall distribution of the high-ratio gas in eastern OMC1 is similar to that of the CN and C_2H molecules, which are both sensitive to the presence of UV radiation (Ungerechtset al. 1997; Melnick et al. 2011). Therefore, the higher temperatures in the eastern OMC1 could be due to external UV heating from the high-mass stars in M42 (e.g. θ^1Ori C) and M43 (e.g. NU Ori). In addition, it is likely that the dense gas in the filaments could block the external radiation, which may explain why the filament regions have high densities and lower temperatures.

We also investigated the gas kinematics inside the two prominent filaments with core fragmentation (labeled 'E' and 'M' in Figure 1a). We found that one of the filaments (E) shows interesting oscillation patterns along its major axis in both intensity and velocity fields (Figure 3). The intensity and velocity peaks toward two of the cores reveal positional shifts of ~λ/4, which is indicative of inflowing gas motions toward these cores (Hacar & Tafalla 2011). Therefore, it is possible that core formation is still ongoing in this filament. On the other hand, similar features were not observed in the other filament (M), where evidences of young protostars have been reported (e.g. Teixeira et al. 2016). It is thus likely that filament

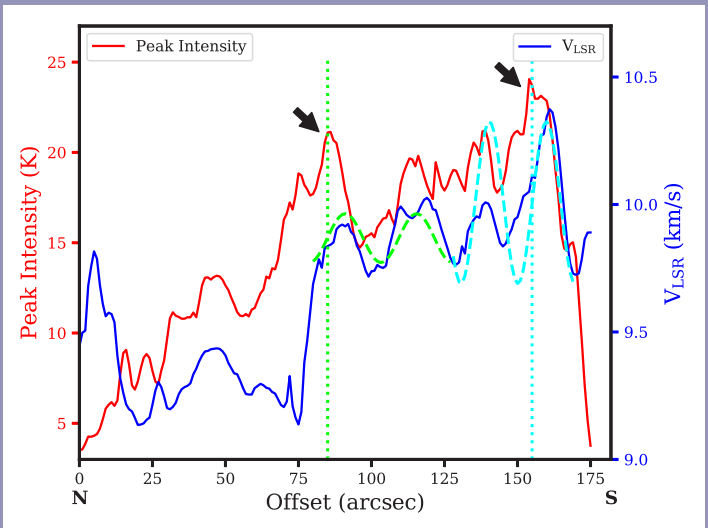

Figure 3: Intensity and velocity variations along the major axis of filament E labeled in **Figure 1a.** The arrows indicate two intensity peaks showing positional shifts relative to their velocity peaks; the dashed curves are sinusoidal fits to the velocity variation, and the two vertical lines show the locations shifted by λ/4 from the fitted sinusoidal peaks of the two cores. Offset 0 is at the northernmost position of this filament.

E is in an earlier evolutionary phase than filament M with star formation signature.

In conclusion, our high-resolution N_2H^+ 3–2 image obtained by combining the SMA and SMT data reveals that OMC1 is a bundle of dense gas filaments. Dense gas in this region is collapsing globally toward the high-mass star-forming region, Orion Nebula Cluster. The eastern part of OMC1 is heated externally from high-mass stars in M42 and M43. Nevertheless, the gas in the filaments remains cold thanks to the shielding from the external heating due to high density. The signature of core-forming gas motions, which is similar to that found in low-mass star-forming regions, is also found in one of the filaments with core fragmentation. Further details of this work are presented in Teng & Hirano (2020).

REFERENCES

- André, P., Di Francesco, J., Ward-Thompson, D., et al. 2014, in Protostars and Planets VI, ed. H. Beuther et al. (Tucson, AZ: Univ. Arizona Press), 27
- Bally, J., Langer, W. D., Stark, A. A., & Wilson, R. W. 1987, ApJ, 312, L45
- Hacar, A., Alves, J., Tafalla, M., & Goicoechea J. R. 2017, A&A, 602, L2
- Hacar, A., & Tafalla, M. 2011, A&A, 533, A34
- Hacar, A., Tafalla, M., Forbrich, J., et al. 2018, A&A, 610, A77
- Koch, E. W., & Rosolowsky, E. W. 2015, MNRAS, 452, 3435
- Melnick, G. J., Tolls, V., Snell, R. L. et al. 2011, ApJ, 727, 13
- Menten, K. M., Reid, M. J., Forbrich, J., & Brunthaler, A. 2007, A&A, 474, 515
- Pattle, K., Ward-Thompson, D., Berry, D. et al. 2017, ApJ, 846, 122
- Peretto, N., Fuller, G. A., Duarte-Cabral, A., et al. 2013, A&A, 555, A112
- Schneider, S. & Elmegreen, B. G. 1979, ApJS, 41, 87
- Teixeira, P. S., Takahashi, S., Zapata, L. A. & Ho, P. T. P., 2016, A&A, 587, A47
- Teng, Y.-H., & Hirano, N. 2020, ApJ, 893, 63
- Ungerechts, H., Bergin, E. A., Goldsmith, P. F. et al. 1997, ApJ, 482, 245
- Van der Tak, F. F. S., Black, J. H., Schoier, F. L., et al. 2007, A&A, 468, 627
- Williams, J. P., de Geus, E. J., & Blitz, L. 1994, ApJ, 428, 693
- Wiseman, J., & Ho, P. T. P. 1998, ApJ, 502, 676

CMZOOM: SURVEY OVERVIEW AND FIRST DATA RELEASE

Newsletter article by Daniel Walker, based on the publication from: Cara Battersby (University of Conn/CfA), Eric Keto (CfA), Daniel Walker (Joint ALMA Observatory/ NAOJ), Ashley Barnes (AIfA University Bonn), Daniel Callanan (CfA/ARI, Liverpool John Moores University), Adam Ginsburg (University of Florida), H Perry Hatchfield (University of Conn), Jonathan Henshaw (MPIfR), Jens Kauffman (MIT/Haystack), J. M. Diederik Kruijssen (University Heidelberg), Steven N. Longmore (ARI, Liverpool John Moores University), Xing Lu (NAOJ), Elisabeth A. C. Mills (University of Kansas), Thushara Pillai (Boston University), Qizhou Zhang (CfA), John Bally (University of Colorado), Natalie Butterfield (Green Bank Obser), Yanett A. Contreras (Leiden University), Luis C. Ho (Peking University), Jürgen Ott (NRAO), Nimesh Patel (CfA) , Volker Tolls (CfA)

Background

The Central Molecular Zone (CMZ, inner ~500 pc of the Galaxy) is an extreme star-forming environment relative to the disk of the Milky Way, with higher gas temperatures (e.g. Güsten et al. 1985; Mills & Morris 2013; Ginsburg et al. 2016; Krieger et al. 2017), greater densities (e.g. Güsten & Henkel 1983; Walmsley et al. 1986; Mills et al. 2018b), elevated turbulence (e.g. Shetty et al. 2012; Kauffmann et al. 2017a; Henshaw et al. 2019), richer chemistry (e.g. Requena-Torres et al. 2006; Requena-Torres et al. 2008; Armijos-Abendaño et al. 2015; Zeng et al. 2018), and stronger magnetic fields (e.g. Crutcher et al. 1996; Pillai et al. 2015). The gas is also subject to an intense UV background field (e.g. Lis et al. 2001; Goicoechea et al. 2004; Clark et al. 2013), elevated cosmic ray ionization rates (e.g. Oka et al. 2005; Goto et al. 2013; Harada et al. 2015; Padovani et al. 2020), X-ray flares (e.g. Terrier et al. 2010, 2018), and dynamical stresses like shearing and compression due to the bar potential (e.g. Güsten & Downes 1980; Longmore et al. 2013a; Krumholz et al. 2017; Kruijssen et al. 2019). The CMZ therefore provides an ideal testbed for probing the effect of environmental conditions on the process of star formation. While such conditions are uncommon in the present day (found locally only in other galactic centers), they may be more typical of gas in galaxies in the early universe, at the peak of cosmic star formation (Kruijssen & Longmore 2013), and may therefore be more cosmologically representative. At a distance of only 8.1 kpc (Reid et al. 2019), the CMZ can serve as a local analog to such star-forming environments, where we are able to study the process of star formation from Galactic-scale flows, down to the scales of protoplanetary disks.

In terms of its current star formation, the CMZ contains a substantial reservoir of molecular gas (3×10^7 $M_\odot$, ~4% of all the molecular gas in the Milky Way; Dahmen et al. 1998), yet the measured star formation rate (SFR) is at least one order of magnitude lower than would be expected given the high density of the gas (Longmore et al. 2013b). This relative dearth of star formation is observed both on global scales and on the scales of individual molecular clouds in the CMZ (Barnes et al. 2017; Lu et al. 2019b). The currently favored explanation for this discrepancy is tied to the gas dynamics, particularly the turbulence of CMZ gas (Kruijssen et al. 2014;

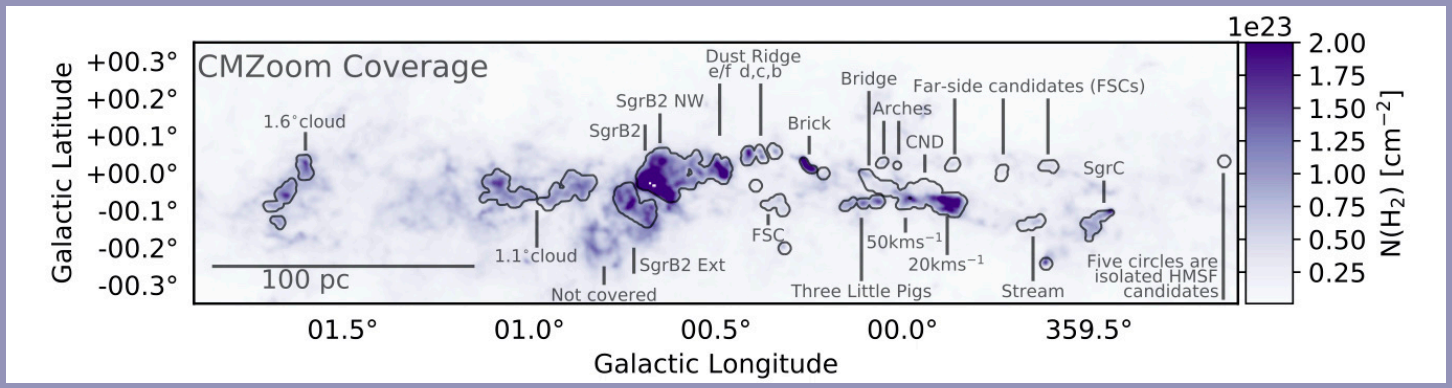

Figure 1: The Central Molecular Zone as seen in $N(H_2)$ derived from the Herschel cold dust continuum (Molinari et al. 2010; Battersby et al. in prep.) in units of cm^{-2} is shown in the colorscale, with the *CMZoom* coverage shown as gray contours. The figure shows colloquial names or notes on each observed region, as they are referred to in Battersby et al. (2020). Within the inner 5° (longitude) x 1° (latitude) of the Galaxy, CMZoom is complete above a column density threshold of 10^{23} cm^{-2}, with the exception of the cloud to the SE of Sgr B2 and isolated bright pixels, and with the addition of a few clouds as noted in Battersby et al. (2020). CMZoom covered 974 individual mosaic pointings over about 550 hours on the SMA.

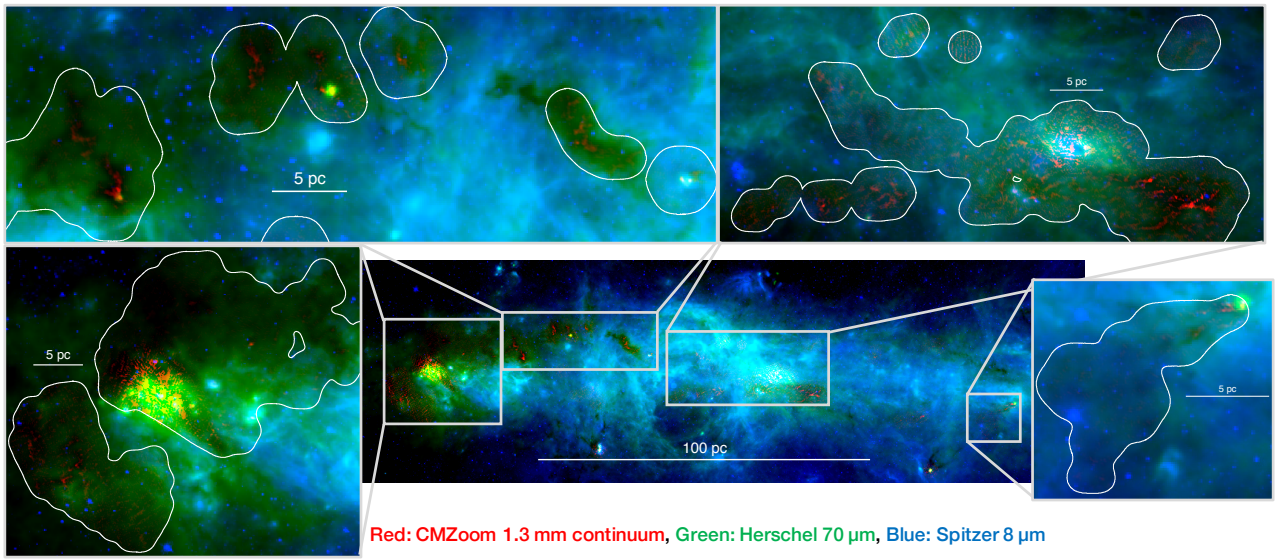

Figure 2: Three color images of the inner ~ 200 pc of the Galaxy, highlighting new *CMZoom* data in red, with various zoom-in views towards regions of interest. This figure shows only part of the full *CMZoom* coverage, which extends in longitude in both directions. All figures show *CMZoom* 1.3 mm dust continuum in red (not primary beam corrected) with survey coverage contours in white. Also shown is Herschel Hi-GAL 70 μm in green (Molinari et al. 2010), and Spitzer GLIMPSE 8 μm in blue (Benjamin et al. 2003). The full image gallery can be found in Battersby et al. (2020).

Rathborne et al. 2014). CMZ turbulence has a greater amplitude at a fixed size-scale and a greater degree of non-compressive motions than in nearby star forming regions, which provides additional support against gravitational collapse (e.g. Krumholz & McKee 2005; Padoan & Nordlund 2011; Federrath et al. 2016; Barnes et al. 2017; Kruijssen et al. 2019).

Understanding why the present day SFR is so low, and any potential environmental dependence of the star formation process, requires a direct connection between the environmental properties of the gas and the resulting star formation. This necessitates long-wavelength observations of the dust continuum and spectral lines on sub-pc scales, sufficient to

resolve individual star-forming clumps and cores across the entire CMZ. Recent interferometric observations have succeeded in doing this to an extent, but they have been limited to individual molecular clouds or small groups of clouds due to the expensive nature of such observations. In order to obtain a more comprehensive view of the present-day star formation in the CMZ, we used the SMA to conduct the first large-scale, high- resolution survey of the CMZ at mm wavelengths. This survey (*CMZoom*, Battersby et al. 2017; Battersby et al. 2020) was made possible thanks to the SMA's unique combination of large primary beam, high angular resolution, and large instantaneous bandwidth, and has produced the first unbiased census of sites of high-mass star formation, along with the physical and kinematic properties of the sub-pc scale structure throughout the CMZ.

Summary of observations & data

CMZoom is a Submillimeter Array (SMA) large program and was designed to target all gas in the CMZ above a Herschel column density of 10^{23} cm^{-2} (Battersby et al. 2011, Battersby et al. in prep.). This threshold was chosen as we are primarily interested in the dense, compact substructure of the gas (the most likely sites of star formation), which we expect to find embedded in the highest column density gas. Using the SMA in compact and subcompact configurations, *CMZoom* observed a total area of ~350 arcmin^2 of high-density gas in the inner 5° (longitude) x 1° (latitude) of the Galaxy at 230 GHz (1.3 mm). This was obtained over a total of 61 observing tracks, 45 in compact configuration, and 16 in subcompact, totalling 550 hours over a period of 4 years. The typical angular resolution of the survey is ~3" (0.1 pc), with a largest angular scale of 45" (1.8 pc). The median continuum RMS achieved throughout the survey is 13.5 MJy Sr^{-1} (~3 - 5 mJy beam^{-1}) though this varies from region to region due to their nature (e.g. strong point sources) and/or systematics (e.g. weather conditions, correlator upgrades, number of antennas available).

Figure 1 shows the full *CMZoom* coverage, while Figure 2 shows a three-color image displaying a sample of the 1.3 mm dust continuum data, along with zoom-ins highlighting regions of interest. In addition to the dust continuum, which provides information about the characteristics of the dense clumps and filaments, we also target key spectral lines in the 230 GHz window. These include ^{12}CO, ^{13}CO, C^{18}O, SiO, H_2CO, CH_3CN, CH_3OH, and more, which will be highlighted in a future publication (Callanan et al. in prep.). Combined, these molecular lines are well-suited to trace phenomena such as protostellar outflows, shocks, dense gas, hot cores, etc. The spectral setup evolved over the duration of the survey due to the incremental upgrade from the ASIC correlator (8 GHz bandwidth) to the SWARM correlator (16 GHz bandwidth). Coverage of the aforementioned key spectral lines was maintained throughout this upgrade.

To recover the zero-spacing information, we complement *CMZoom* with single-dish data from the Bolocam Galactic

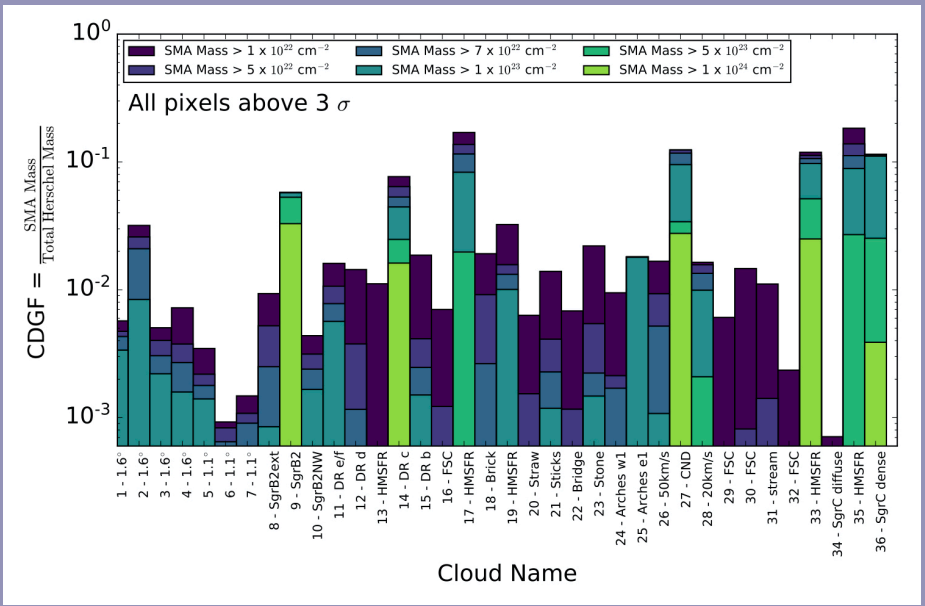

Figure 3: The compact dense gas fraction (CDGF) as measured by comparing the SMA and Herschel mass in each cloud. The names on the x-axis consist of a prefix, which is the mask number, and a shorthand name for each cloud (see Battersby et al. 2020 for details). Regions are ordered in decreasing central Galactic longitude from left to right. Each bar shows the mass above 3σ in the corresponding *CMZoom* (SMA) cloud, above various column density thresholds as shown in the legend, divided by the total mass of the cloud (at all column densities) as seen in Herschel. The overall CDGF is less than 10% for most of the clouds, but this figure demonstrates the varying levels of substructure in each cloud. Note that the apparently high CDGF seen toward the CND located near l = 0° is likely due to contamination from the strong synchrotron source Sgr A* and resulting imaging artifacts.

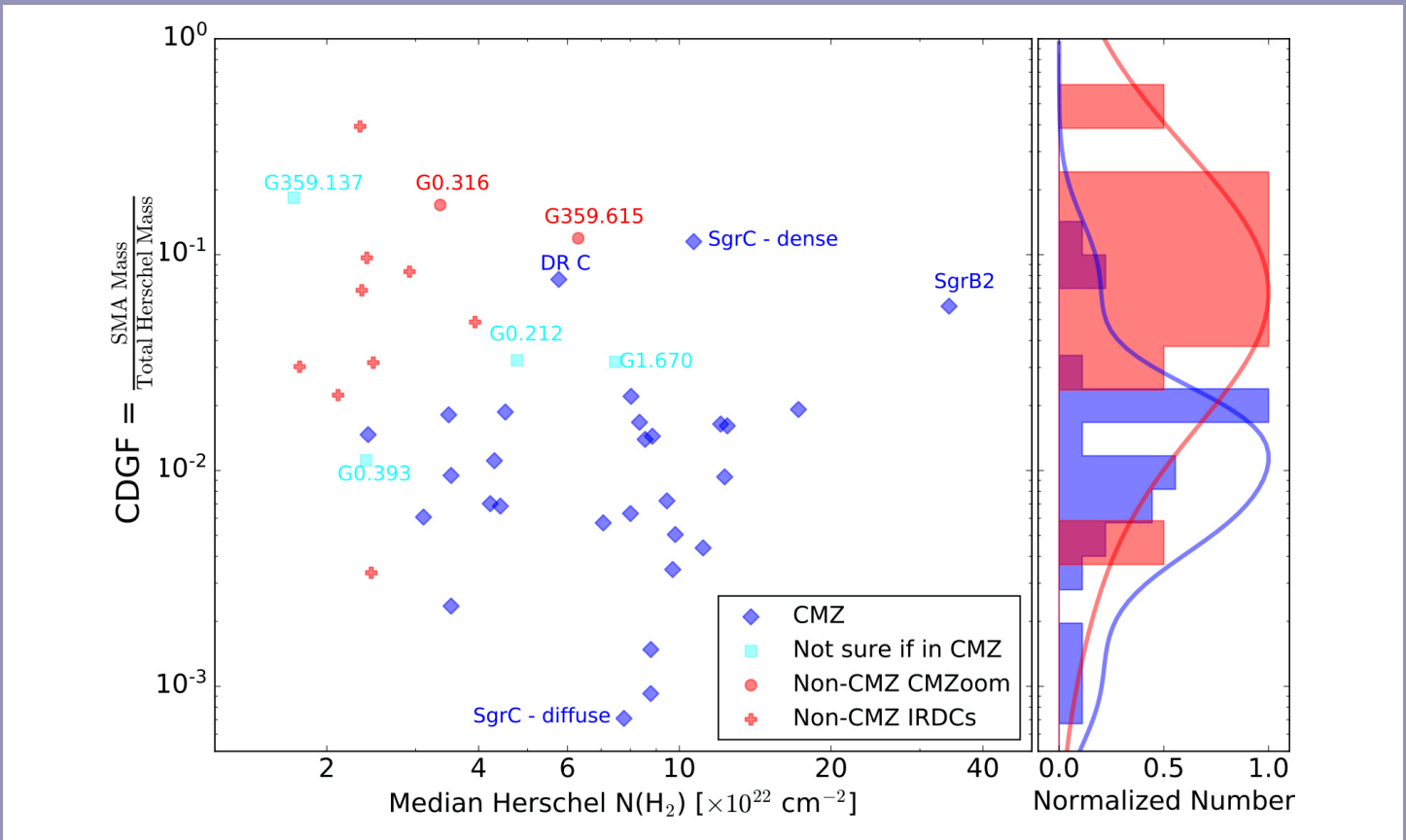

Figure 4: Clouds in the CMZ overall have a much lower compact dense gas fraction (CDGF), with the exception of highly star-forming regions (Dust Ridge Cloud C, SgrC - dense, and SgrB2), than clouds in the Galactic disk, despite their high average column densities. This figure shows the CDGF, which is calculated as the SMA mass divided by the Herschel mass for each cloud. The right panel shows the histogram of CMZ (blue) and non-CMZ (red) data points with a Kernel Density Estimator fit. Clouds marked with a dark blue diamond are located within the CMZ, those marked with cyan squares have uncertain distances, and those marked as red circles, plus signs, or an x are not in the CMZ. While we tried to measure the CDGF and median column density for the non-*CMZoom* points in the same way, we advise a factor of two uncertainty in the interpretation of the relative data points.

Plane Survey (BGPS, dust continuum; Bally et al. 2010; Aguirre et al. 2011; Ginsburg et al. 2013) and an APEX spectral line survey of the CMZ (Ginsburg et al. 2016).

A lack of dense compact sources in the CMZ

Understanding why the SFR in the CMZ is currently so low is crucial in developing our understanding of how star formation varies as a function of environment. *CMZoom* provides a uniquely comprehensive view, allowing us to address this question on sub-pc scales throughout the CMZ to determine whether compact cores have difficulty collapsing into stars, or whether the gas in the CMZ does not efficiently produce such cores in the first place.

In order to distinguish between these scenarios, we require a way to quantify the compact substructure within the CMZ gas clouds that also enables a direct comparison with similar measurements in other environments. The 'dense gas fraction' is commonly used in the literature to describe the degree of substructure in gas clouds. However, this cannot be used because the definition of "dense" is ambiguous, and the mean density of CMZ clouds (~10^4 cm^{-3}) lies at or above the threshold used to define "dense" substructure in most studies. We therefore define the term 'Compact Dense Gas Fraction' (CDGF) as a measurement of the fraction of a cloud's mass that is contained in over-densities on 0.1 - 2 pc scales.

To compute the CDGF, we sum the mass of compact structures above 3σ in each cloud recovered by the SMA, and divide that by the total mass of the cloud recovered by Herschel, using the same Herschel column density map which informed our source selection for the survey. The resulting CDGFs for each survey region are shown in Figure 3. Each region (a bar on the x-axis) is split up into how much of the recovered SMA mass originates at each of the labelled SMA column densities. This shows that the CDGFs are typically low

(< 10%), and that two regions can have similar overall CDGFs, but with gas that is substructured in very different ways. For example, G1.670−0.130 (cloud 2) and G0.699−0.028 (Sgr B2, cloud 9) have similar overall CDGFs (3% and 6%, respectively), yet the highest column density gas in G1.670−0.130 is 10^{23} cm^{-2} while much of the gas in Sgr B2 is closer to 10^{24} cm^{-2}.

In Figure 4, we plot the CDGFs vs. the mean column density for each survey region. We also plot the same parameters for a sample of Infrared Dark Clouds (IRDCs) in the Galactic disk for comparison. This shows that while the majority of the CMZ clouds are at higher global column densities, their CDGFs are typically lower than those in IRDCs in the Galactic disk. In the few cases where the CDGFs of CMZ clouds are similar to those in the disk IRDCs, they are actively star-forming regions (i.e. Sgr B2, DR C, Sgr C-dense).

A key first result of the *CMZoom* survey is that there is an overall deficit of compact substructure in CMZ clouds on 0.1 - 2 pc scales, both qualitatively (Figure 2) and as measured by low CDGFs (Figures 3 & 4). Where the CDGF is high (i.e. similar to typical values in star-forming regions in the Galactic disk), the regions are actively star-forming. We therefore conclude that the comparatively low star formation efficiency of high column density clouds in the CMZ is likely a direct result of the inability of this gas to fragment into compact substructures. Where these compact substructures do form, star formation seems to proceed as expected. This is a crucial addition to the growing body of evidence showing that the CMZ rules out a universal density threshold for star formation (which needs to be much higher than elsewhere in the Galactic disk) or a universal star formation efficiency per free-fall time (which needs to be much lower in CMZ clouds with a low CDGF).

Looking to the future

Here we have provided an overview of the *CMZoom* survey, and some of the first results from the continuum data. A more detailed discussion of these data, additional methods, and associated uncertainties can be found in Battersby et al. (2020). The continuum source catalog will soon be published in a companion paper by Hatchfield et al. (submitted), which will detail the locations and properties of the hundreds of compact continuum sources detected. This catalog, constructed using a pruned dendrogram algorithm, identifies and characterizes more than 95% of compact sources with masses above 80 $M_{\odot}$, and is more than 95% complete for all possible precursors of high mass star formation in the CMZ embedded in gas above 10^{23} cm^{-2}. In this upcoming work we also place an upper limit on the star formation potential of the CMZ within the next 10^{4-5} years. Molecular line data will be presented in an upcoming publication by Callanan et al. (in prep.).

The calibrated SMA datasets and reduced continuum images are publicly available on the *CMZoom* Dataverse and the SMA Data Archive (along with the raw data). We will also release the fully imaged sidebands and molecular line cubes with the publication of Callanan et al. (in prep.) in the near future.

REFERENCES

- Aguirre, J. E., Ginsburg, A. G., Dunham, M. K., et al. 2011, ApJS, 192, 4
- Armijos-Abendaño, J., Martín-Pintado, J., Requena-Torres, M. A., et al. 2015, MNRAS, 446, 3842
- Bally, J., Anderson, L. D., Battersby, C., et al. 2010, A&A, 518, L90
- Barnes, A. T., Longmore, S. N., Battersby, C., et al. 2017, MNRAS, 469, 2263
- Battersby, C., Bally, J., Ginsburg, A., et al. 2011, A&A, 535, A128
- Battersby, C., Keto, E., Zhang, Q., et al. 2017, in IAU Symposium Vol. 322, 90
- Battersby, C., et al. 2020, accepted to ApJ, eprint arXiv:2007.05023
- Benjamin, R. A., Churchwell, E., Babler, B. L., et al. 2003, PASP,115, 953
- Clark, P. C., Glover, S. C. O., Ragan, S. E., Shetty, R., & Klessen, R. S. 2013, ApJL, 768, L34
- Crutcher, R. M., Roberts, D. A., Mehringer, D. M., & Troland, T. H. 1996, ApJL, 462, L79
- Dahmen, G., Huttemeister, S., Wilson, T. L., & Mauersberger, R. 1998, A&A, 331, 959
- Federrath, C., Rathborne, J. M., Longmore, S. N., et al. 2016, ApJ, 832, 143
- Ginsburg, A., Glenn, J., Rosolowsky, E., et al. 2013, ApJS, 208, 14
- Ginsburg, A., Henkel, C., Ao, Y., et al. 2016, A&A, 586, A50
- Goicoechea, J. R., Rodríguez-Fernández, N. J., & Cernicharo, J. 2004, ApJ, 600, 214
- Goto, M., Indriolo, N., Geballe, T. R., & Usuda, T. 2013, Journal of Physical Chemistry A, 117, 9919
- Güsten, R., & Downes, D. 1980, A&A, 87, 6
- Güsten, R., & Henkel, C. 1983, A&A, 125, 136
- Güsten, R., Walmsley, C. M., Ungerechts, H., & Churchwell, E. 1985, A&A, 142, 381
- Harada, N., Riquelme, D., Viti, S., et al. 2015, A&A, 584, A102
- Henshaw, J. D., Ginsburg, A., Haworth, T. J., et al. 2019, MNRAS, 485, 2457
- Kauffmann, J., Pillai, T., Zhang, Q., et al. 2017a, A&A, 603, A89
- Krieger, N., Ott, J., Beuther, H., et al. 2017, ApJ, 850, 77

- Kruijssen, J. M. D., & Longmore, S. N. 2013, MNRAS, 435, 2598
- Kruijssen, J. M. D., Longmore, S. N., Elmegreen, B. G., et al. 2014, MNRAS, 440, 3370
- Kruijssen, J. M. D., Dale, J. E., Longmore, S. N., et al. 2019, MNRAS, 484, 5734
- Krumholz, M. R., & McKee, C. F. 2005, ApJ, 630, 250
- Krumholz, M. R., Kruijssen, J. M. D., & Crocker, R. M. 2017, MNRAS, 466, 1213
- Lis, D. C., Serabyn, E., Zylka, R., & Li, Y. 2001, ApJ, 550, 761
- Longmore, S. N., Kruijssen, J. M. D., Bally, J., et al. 2013a, MNRAS, 433, L15
- Longmore, S. N., Bally, J., Testi, L., et al. 2013b, MNRAS, 429, 987
- Lu, X., Zhang, Q., Kauffmann, J., et al. 2019b, ApJ, 872, 171
- Mills, E. A. C., & Morris, M. R. 2013, ApJ, 772, 105
- Mills, E. A. C., Ginsburg, A., Immer, K., et al. 2018b, ApJ, 868, 7
- Molinari, S., Swinyard, B., Bally, J., et al. 2010, A&A, 518, L100
- Oka, T., Geballe, T. R., Goto, M., Usuda, T., & McCall, B. J. 2005, ApJ, 632, 882
- Padoan, P., & Nordlund, Å. 2011, ApJ, 730, 40
- Padovani, M., Ivlev, A. V., Galli, D., et al. 2020, SSRv, 216, 29
- Pillai, T., Kauffmann, J., Tan, J. C., et al. 2015, ApJ, 799, 74
- Rathborne, J. M., Longmore, S. N., Jackson, J. M., et al. 2014, ApJL, 795, L25
- Reid, M. J., Menten, K. M., Brunthaler, A., et al. 2019, ApJ, 885, 131
- Requena-Torres, M. A., Martín-Pintado, J., Martín, S., & Morris, M. R. 2008, ApJ, 672, 352
- Requena-Torres, M. A., Martin-Pintado, J., Rodríguez-Franco, A., et al. 2006, A&A, 455, 971
- Shetty, R., Beaumont, C. N., Burton, M. G., Kelly, B. C., & Klessen, R. S. 2012, MNRAS, 425, 720
- Terrier, R., Ponti, G., Bélanger, G., et al. 2010, ApJ, 719, 143
- Terrier, R., Clavel, M., Soldi, S., et al. 2018, A&A, 612, A102
- Walmsley, C. M., Güsten, R., Angerhofer, P., Churchwell, E., & Mundy, L. 1986, A&A, 155, 129
- Zeng, S., Jiménez-Serra, I., Rivilla, V. M., et al. 2018, MNRAS, 478, 2962

BEYOND OUR LOCAL HORIZON: DUST CONTINUUM OBSERVATIONS OF INDIVIDUAL GIANT MOLECULAR CLOUDS ACROSS ANDROMEDA'S NEIGHBORHOODS

Jan Forbrich (U Hertfordshire, CfA), Charlie Lada (CfA), Sébastien Viaene (U Ghent), Glen Petitpas (CfA), Chris Faesi (UMass Amherst), and Jonathan Toomey (U Hertfordshire)

As we approach the centenary of Edwin Hubble's discovery that the Andromeda Nebula was not actually comparable to the Orion Nebula but instead an entire galaxy in its own right, the SMA is providing us with a new perspective on our cosmic neighbour – and it is helping us to place local star formation, including in fact the Orion Nebula, into a wider context. The key here is the unprecedented ability of the upgraded SMA to detect the faint dust continuum emission of individual giant molecular clouds (GMCs) in the Andromeda Galaxy – in fact, the first resolved detection of dust emission toward extragalactic GMCs beyond the Magellanic Clouds.

Star formation plays a critical role in both galaxy and cosmic evolution. Indeed, it is the rate of star formation that is the primary metric for cosmic evolution studies (e.g., Madau & Dickinson 2014). Within galaxies star formation occurs in GMCs. The physical conditions within these clouds set the star formation rate (SFR) for both the clouds and the galaxies which contain them. Understanding the physical nature of GMCs is thus key to understanding the physical processes that drive star formation, set the SFR and thus control the evolution of galaxies.

Molecular clouds are composed almost entirely of molecular hydrogen (H^2) gas. However, H^2 is generally unobservable because its lowest rotational energy levels are too high above the ground state to be collisionally excited at the temperatures (10-30K) characteristic of molecular clouds. Moreover, it lacks a permanent dipole moment rendering any such rotational transitions extraordinarily weak in the first place. Traditionally, molecular clouds have been traced by observations of CO which, despite the fact that it is the next most abundant molecular species, contributes only ~0.03% to the total molecular cloud mass. However, variations in CO abundances, opacities and excitation conditions within and between clouds greatly complicate interpretation of these observations.

After decades of slow progress in Milky Way molecular cloud research dominated by observations of rare gas traces like CO, the field was transformed when observational capabilities were developed that enabled reliable measurements of the *dust* in GMCs, which accounts for 1% of total cloud masses (~30 times that contributed by molecular lines). Near-infrared, wide-field imaging surveys produced exquisite dust extinction maps of nearby clouds providing unprecedented data on cloud structure and the first robust and consistently reliable masses of local GMCs (e.g., Lada et al. 1994; Alves et al. 2001; Lombardi et al. 2010; Goodman et al. 2009). The *Herschel* and *Planck* missions have produced wide-area surveys of dust continuum emission greatly improving on the sensitivity, resolution and dynamic range of dust (and total) column density measurements in Milky Way GMCs (e.g., Lombardi et al. 2014, André et al. 2010).

Measurements of dust column densities are not hampered by considerations of excitation, chemistry (e.g., depletion) and opacity that severely hinder measurements of molecular-line column densities. At the same time comparisons of molecular-line and dust measurements have provided

more direct and accurate determinations of molecular abundances and excitation than provided by modelling of the line emission alone, significantly improving our understanding of cloud chemistry (e.g., Bergin et al. 2002). In contrast, measurements of dust column densities using dust continuum observations depend primarily on the dust opacity and temperature, where both parameters have been constrained to an unprecedented degree due to the *Planck* and *Herschel* missions. With knowledge of the well-constrained gas-to-dust mass ratio, measurements of dust emission result in lower uncertainties for cloud mass estimates.

Measurements of resolved dust emission in a population of GMCs in an external galaxy would produce a wealth of information about the fundamental properties of the GMC population including, for example, a robust determination of the GMC mass function. Such a determination would significantly improve on Milky Way results which are hampered by the small numbers of GMCs for which reliable and accurate cloud distances are known. This issue is minimized in an external galaxy where all GMCs are at the same relative distance from the Sun.

Until now resolved dust continuum measurements of extragalactic GMCs have not been possible because no telescopic facility had the combined sensitivity and angular resolving power to enable such observations. The recent addition of wide-band continuum receivers to the SMA instrument suite is now enabling, for the first time, resolved measurements of dust emission in individual GMCs within the nearest spiral galaxy, M31, the famous Andromeda galaxy.

It was in M31 that individual extragalactic GMCs were first resolved, using CO observations and an earlier generation of millimeter-wavelength observatories (Vogel et al. 1987, Lada at al. 1988). Now, the powerful combination of SMA sensitivity and the proximity of M31 make dust continuum observations feasible. Moreover, CO emission can be excised from the bandpass enabling a "clean", uncontaminated measurement of the dust emission. The excised CO spectra can then be utilized separately producing a powerful set of simultaneous observations of both tracers.

The spatial sensitivity of the SMA is perfectly geared toward studies of GMCs in M31. Starting with the subcompact con-

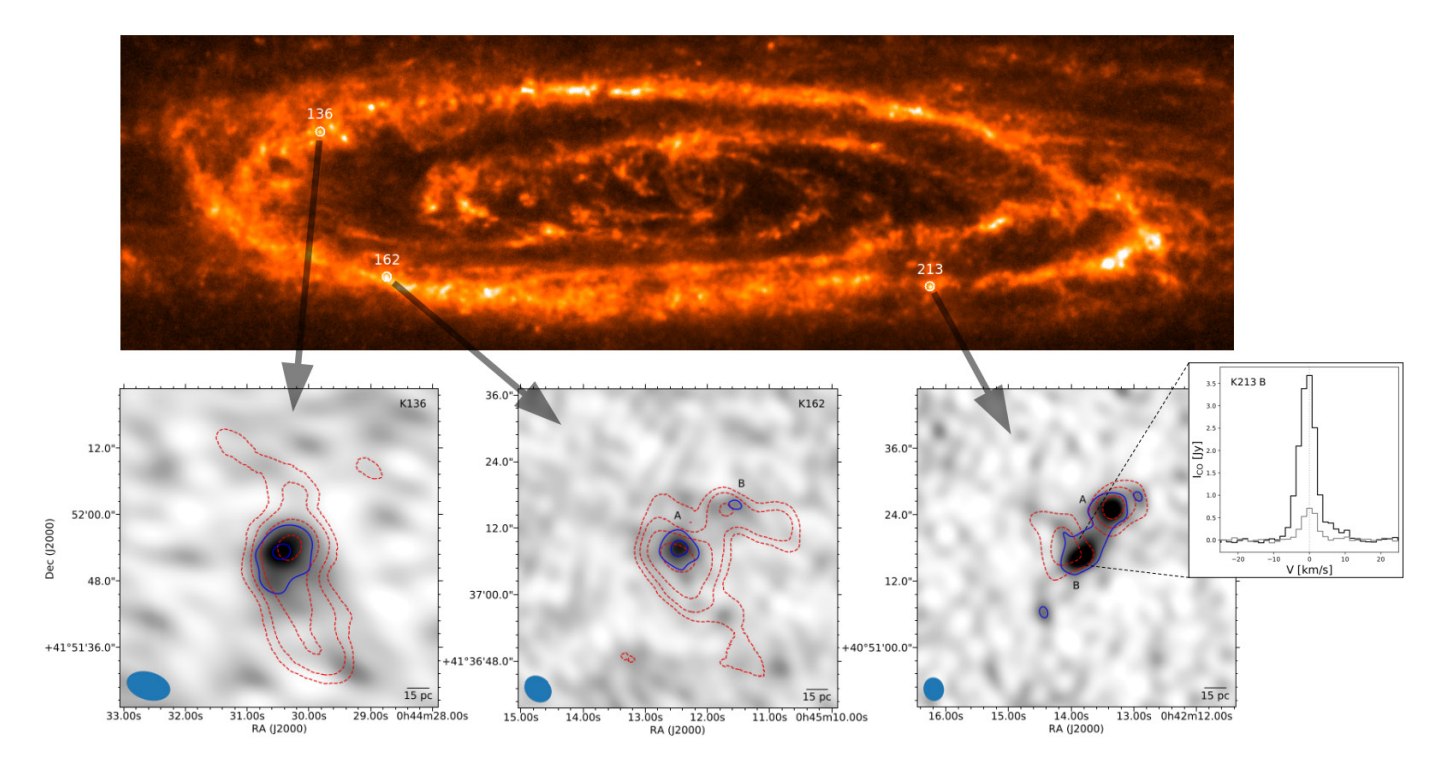

Figure 1: Three examples of dust detections (greyscale) of individual GMCs in M31, from left to right: K162, K136, and K213 (referring to Kirk et al. 2015), as indicated in the above Herschel 350 micron image, with circles the size of the SMA 230 GHz primary beam. The blue contours show the 3σ and 6σ levels of the dust continuum while the red dashed contours show the ^{12}CO(2-1) moment 0 map, at levels of 6σ, 12σ, 24σ, etc. The sub-panel on the right-hand side shows an example of a ^{12}CO(2-1) (black) and even ^{13}CO(2-1) (grey) spectrum for an individual GMC, K213B. Excerpted and adapted from Forbrich et al. (2020).

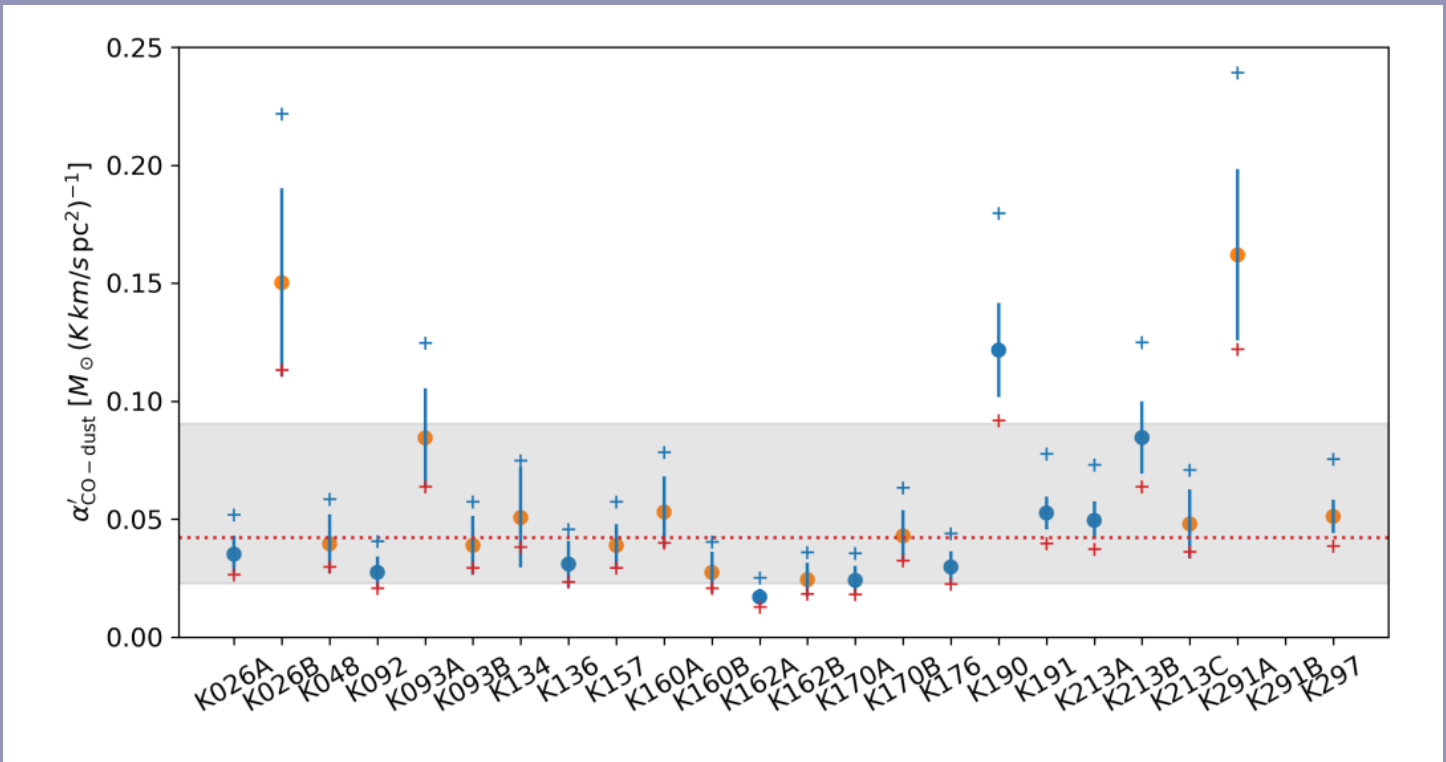

Figure 2: Direct $\alpha'_{CO\text{-}dust}$ measurements per cloud, converting CO luminosity to dust mass. Blue dots indicate resolved sources, and orange dots indicate unresolved sources, both for T = 20 K. Red and blue crosses additionally show $\alpha'_{CO\text{-}dust}$ for T = 25 K and T = 15 K, respectively. The dotted line indicates the sample mean of $\alpha'_{CO\text{-}dust}$ = 0.042 M_{solar}/(K km/s/pc^2). For comparison, we divide the nominal Galactic value for the CO(2-1) transition by a gas-to-dust ratio of 136 to find a near-identical value of $\alpha'_{CO\text{-}dust(Gal)}$ = 0.045 M_{solar}/(K km/s/pc^2), and we indicate the corresponding range with an uncertainty of ±0.3 dex as a gray-shaded area. Note that K291B is off-scale. From Forbrich et al. (2020).

figuration, the synthesized beam at 230 GHz has an absolute size of ~15pc, which is perfect to resolve GMCs of sizes ~50–100pc. The primary beam size at 230 GHz corresponds to an absolute field of view of ~200pc, which is well-matched to observations of GMCs.

Unfortunately, the Andromeda Galaxy is far too large in angular extent in the sky for even large sections to be fully mapped by the SMA; it is important to know where to look. Important groundwork in this regard has been laid by the *Herschel Space Observatory*, which has been used to map the entire galaxy. In particular, a catalog of its Giant Molecular Associations (GMAs) at scales of ~90 pc has been obtained by Kirk et al. (2015), enabling us to target locations where GMAs could be resolved into individual GMCs.

After a successful pilot experiment, we are currently conducting a Large Scale program with the SMA to build a statistically meaningful sample of 100 GMCs in M31 with resolved dust continuum and CO detections. Even with the wideband upgrade, about one full track per source is required to obtain reliable dust continuum detections, but we find that with one full track we detect individual GMCs in the vast majority of targeted GMAs. The main goal of our survey is to use resolved dust continuum measurements to place the fundamental measurements of GMC masses and sizes, across the disk of M31, on the same footing as studies of local clouds in the Milky Way. With ^{12}CO(2-1), ^{13}CO(2-1), and C^{18}O(2-1) in the bandpass and available for analysis with the same calibration, (*u,v*) coverage, and astrometry as the dust, the resulting sample will provide a unique comparison of dust and gas in GMCs within and throughout an entire spiral galaxy.

In our first paper (Forbrich et al. 2020), we describe an initial investigation of the GMC population in M31, mainly based on the portion of the sample observed in the first season (with a total of 24 individual detections toward 16 GMAs, of which nine were resolved). This investigation highlights the new capabilities of the SMA. In Figure 1, we show an example of GMCs detected in both dust continuum and CO, and we include an example spectrum in ^{12}CO(2-1) and even ^{13}CO(2-1) for an individual cloud.

In this first paper, we also demonstrate the link to Galactic science by using simulated observations of what Orion A, a very average-sized Milky Way GMC, would look like if placed in M31 and observed with the SMA. Amazingly, the simulations predict that a significant fraction (10-20%) of the dust emitting area of Orion A can be detected in a single track with the sub-compact and compact configurations under good atmospheric conditions (1-2 mm pwv). At the same time, a direct comparison with the full extent of the cloud can be made using ^{12}CO(2-1), detected at a S/N ratio of several 100, allowing us to detect the full GMC extent and to quantitatively assess the fraction of the cloud seen in dust emission – while also helping to identify contamination from emission unrelated to clouds, for example from background galaxies. This game-changing capability will improve even further with the continuing wideband upgrade. For example, with the full upgraded bandwidth (64 GHz), under very good atmospheric conditions (1 mm pwv), 80% of the entire dust emitting area of Orion A would be detected in a single track!

As a first science result, we have used the simultaneously obtained dust continuum and ^{12}CO(2-1) data to measure the CO X-factor (or, alternatively, α_{CO}). This parameter is used to convert a CO detection to a total gas mass. Such measurements are essential to justify the use of CO integrated intensity for cloud mass measurements when dust cannot be independently detected. In our measurements of the conversion factor in M31, a number of common uncertainties are minimized by our use of CO and dust continuum data obtained simultaneously with identical observing conditions, calibration, spatial filtering, and astrometry.

Based on our initial sample, we find that the GMC-scale CO conversion factor in M31 is remarkably constant across the galaxy. Our results are shown in Figure 2, where we show the conversion factor of CO to dust mass, or α'CO. Assuming a standard gas-to-dust ratio of 136, the result is in excellent agreement with the corresponding factor in the Milky Way.

One of our ultimate goals is to study the cloud-scale star formation laws in M31. In order to do so we require as statistically robust a sample as possible and we need reliable cloud-scale star formation rate tracers in addition to GMC metrics. These are notoriously hard to obtain, in marked contrast to the situation for the local Galactic clouds. To remedy this problem we have recently obtained a VLA survey of the centimetric free-free emission from HII regions in the vicinity of all M31 GMAs – a survey that is in turn enabled by the VLA wideband upgrade. These observations are providing us with the highest-resolution, most direct and extinction-free tracer of (high mass) star formation available, enabling the first study of cloud-scale star formation laws in M31. Given the meaningful overlap in scale with corresponding studies of Milky Way clouds, we aim to assess both local and extragalactic scaling relations (e.g., Lada et al. 2012). Furthermore, it will be interesting to see if quiescent GMCs with no apparent star formation can be identified. The in-band CO data will additionally enable a look at Larson's relations for M31 GMCs (Larson 1981).

The SMA is now in a unique position to provide key insights into cloud-scale star formation, bridging the gap between Galactic and extragalactic star formation science and placing both on the same footing. As of the time of writing, we have already obtained a sample that is about a quarter of its intended final size, where the main driver for the upcoming observations in this ongoing program is to build significant subsamples of GMCs in the different environments across M31 and to obtain a well populated overall GMC mass function.

Even with just a partial sample, the unprecedented SMA capabilities are already producing exciting early science results. In our next steps, we are now working on fully incorporating the CO isotopologues in our interpretation of the dust detections. We are additionally preparing the next observing season, in which we will use our VLA survey to further optimize our target selection criteria and to cover an even wider range of star formation environments. Additionally, first pilot observations at 345 GHz will be expanded to obtain constraints on dust properties in selected GMCs. Stay tuned! Dust observations of resolved individual GMCs are now feasible well beyond our local horizon, once again confirming Edwin Hubble's observation that "the history of astronomy is a history of receding horizons".

REFERENCES

- Alves et al. 2001, Nature 409, 159
- André et al. 2010, A&A 518, 192
- Bergin et al. 2002, ApJ 570, 101
- Forbrich et al. 2020, ApJ 890, 42
- Goodman et al. 2009, ApJ 692, 91
- Kirk et al. 2015, ApJ 798, 58
- Lada et al. 1988, ApJ 328, 143
- Lada et al. 1994, ApJ 429, 694
- Lada et al. 2012, ApJ 745, 190
- Lombardi et al. 2010, A&A 519, L7
- Lombardi et al. 2014 , A&A 566, 45
- Madau & Dickinson 2014, ARA&A 52, 145
- Vogel et al. 1987, ApJL 321, 125

THE QUEST TO DESIGN THE wSMA VACUUM WINDOW

Keara Carter & Edward Tong (CfA)

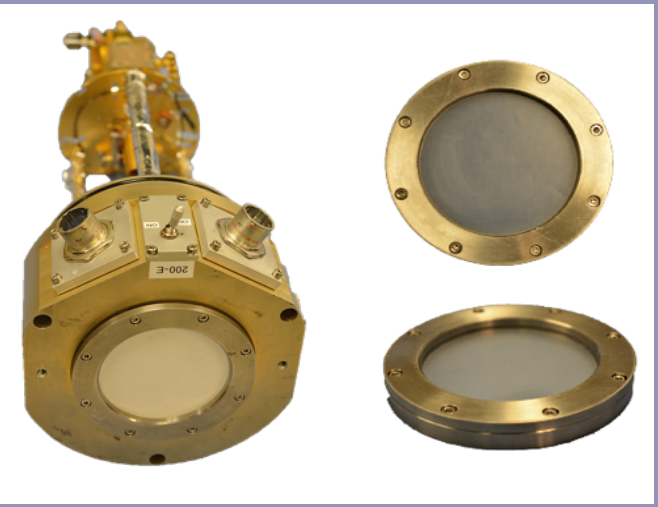

Figure 1: Left – SMA receiver insert. Right – Current SMA vacuum window, polyethylene coated quartz.

Introduction:

A very important and yet often overlooked area in SIS receiver design is that of the vacuum window. A great deal of effort has been spent maximizing the effectiveness of the front-end receiver chain, and yet, one of the first components of this chain, the window through which the astronomical signal enters the cryostat, has received less attention. For the new wSMA receiver package, the size of the cryostat window will be larger than that of the current SMA receiver inserts. The window will also be responsible to transmit a much wider bandwidth. At present, SMA receivers employ crystalline quartz vacuum windows (see Fig. 1) coated with a layer of polyethylene as an anti-reflection coating. If we retain the same type of window for wSMA, we will need a much thicker quartz window and a more elaborate anti-reflection coating. As a result, a new vacuum window design is required in earnest.

Vacuum windows need to be sufficiently strong to endure the large pressure difference between outside air and the vacuum inside the cryostat. They also need to be adequately transparent, to allow the maximum amount of radiation through. While a thick window affords a higher mechanical strength, it also introduces higher optical losses. Clearly, there is a trade-off between mechanical strength and low-losses, and a judicious choice of window material is the key for the design. Newly developed high-strength plastic materials may provide the answer. At the Submillimeter Receiver Lab, we have been investigating the electrical and mechanical properties of many different materials in the quest to create an optimized vacuum window design.

Requirements:

The wSMA receivers feature windows with a clear aperture of 105 mm in diameter, an increase of over 30% from that currently used in SMA receiver inserts. These windows will need to operate with less than 1% loss, while offering a reflection of below -20 dB , over a continuous frequency range of 190 – 380 GHz. Our method has been to first conduct transmission measurements of a variety of materials with a Quasi-Optical Vector Network Analyzer (QO-VNA) to determine their refractive indices and loss tangents. If these values meet our minimum requirements, we then use an SIS (Superconductor-Insulator-Superconductor) mixer to perform an in-situ test using the Method of Intersecting Lines to confirm the measured loss. Our search has been biased towards low-loss materials with low refractive indices, which will facil-

itate the design of anti-reflection coating. Mechanical testing follows, conducted on a vacuum chamber with an aperture diameter close to that of the wSMA upgrade. We have made long duration measurements on the creep behavior of plastic materials by monitoring the deformation of windows placed under vacuum. These tests allow us to gain information on the material's tensile strength and longevity.

Electrical Testing:

Fig. 2 shows the QO-VNA that has been set up in the Receiver Lab. Operating between 210 and 370 GHz, this analyzer allows for the measurement of the complex refractive indices of materials. The material under test is placed on the sample holder, attached to a translation stage located between two 90-degree off-axis parabolic mirrors with focal lengths of 50.8 mm. Efforts are made to ensure the sample is as flat and perpendicular to the incoming wave as possible. A bi-directional coupler on the source side uses harmonic mixers to monitor the amplitude and phase of the incident wave as well as the reflected wave for reflection measurements. The transmitted wave is measured by another harmonic mixer connected to the receiving horn. To reduce back reflections from the receiving horn and harmonic mixer, a reflective neutral density filter, which acts as an attenuator (of -12.5 dB at 300 GHz), is placed between the sample holder and the receiving mirror at a roughly 45 degree angle. Fundamental Gaussian analysis of this setup shows that the beam waist, where the wave front is planar, is located very close to the sample holder. The value of the beam waist radius is about 12 mm.

Transmission measurements are repeated with the material sample in place and with the sample removed. The ratio of these measurements provides a complex transmission coefficient, from which we can extract the refractive index and loss tangent of the material (C.A. Balanis, 1989) (D. Bourreau et al., 2006). Table 1 lists the results for some materials that we have tested.

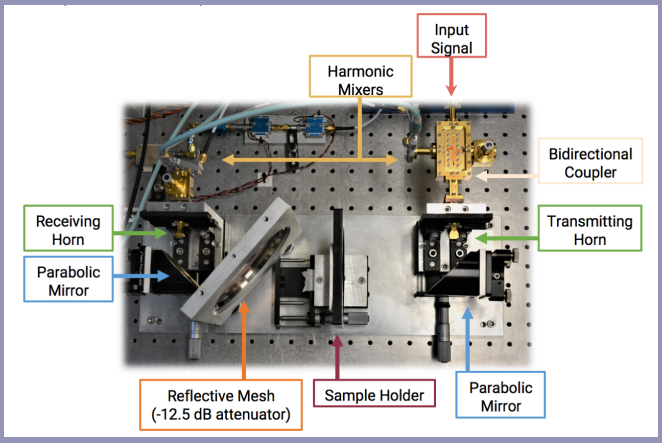

Figure 2: QO-VNA (Quasi-Optical Vector Network Analyzer).

The loss tangent of selected materials measured with the QO-VNA have been confirmed with in-situ loss measurements using the Method of Intersecting Lines with SIS receivers (C.-Y. E. Tong et al., 2008). This procedure involves taking Y-factor measurements using hot and cold loads for a range of Local Oscillator (LO) levels. From this, the equivalent input noise temperature of the RF input section of the receiver can be derived. The difference between the input noise temperature with the additional optics element (the sample) and without yields a measurement of the loss due to the sample, which is accurate down to about 1%. Since this is a more

	Using the QO-VNA			Using the Method of Intersecting Lines	
Material	**Thickness (mm)**	**Refractive index (n)**	$tan\delta\ [\times\ 10^{-3}]$	**Thickness (mm)**	$tan\delta\ [\times\ 10^{-3}]$
High Density Polyethylene (HDPE)	10.15	1.5323	0.6 ± 0.2	2.37	0.9 ± 0.2
Honeywell Spectra (Dyneema)	4.97	1.552	1 ± 0.4	1.84	3.2 ± 0.1
Polypropylene (PP)	6.32	1.5026	0.5 ± 0.3	1.48	0.8 ± 0.2
Polystyrene (PS)	1.27	1.594	2 ± 1.5		
Ultra-High Molecular Weight Polyethylene (UHMW PE)	3.28	1.514	----------		
Z- Cut Crystalline Quartz	4.97	2.107	----------	4.97	0.5 ± 0.1

---------- indicates value is below measurement threshold. Blank spaces indicate no measurement data.

Table 1: Refractive indices and loss tangent (tan δ) of various materials extracted from the measurements using both the QO-VNA and SIS receiver with the Method of Intersecting lines. Note the different thicknesses of materials used with either method.

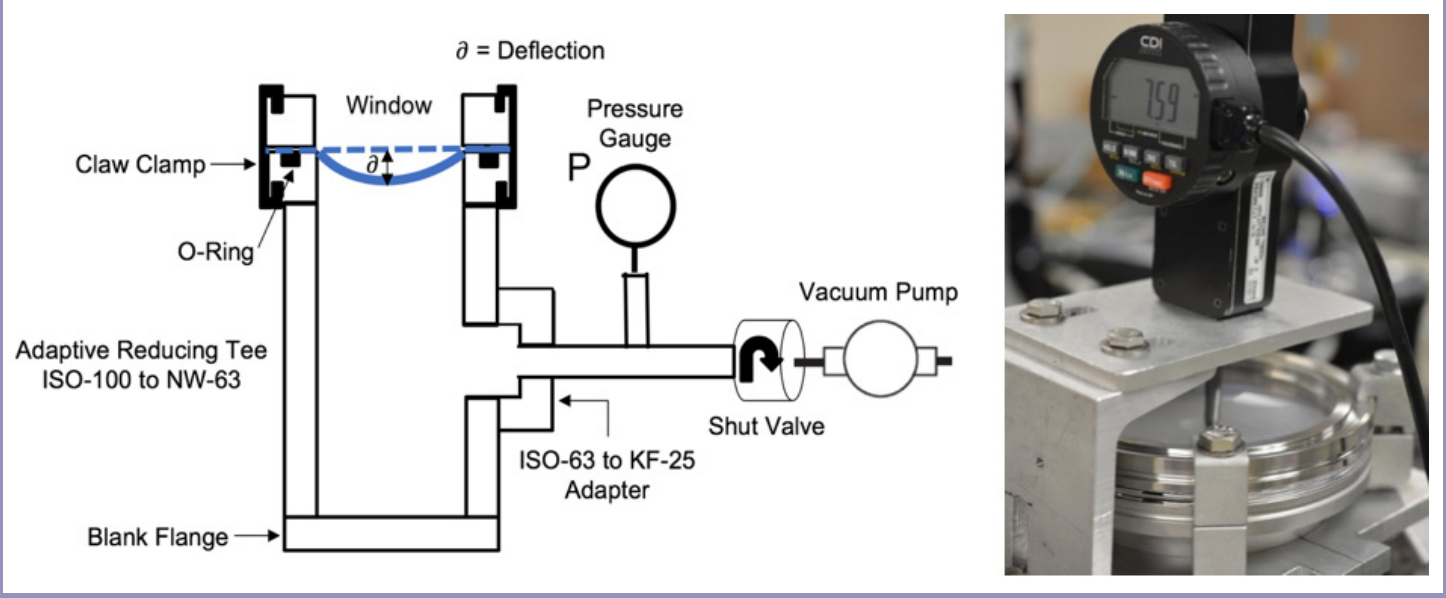

Figure 3: Mechanical window central deflection experimental setup. Left- illustration of full setup. Right- image of the drop indicator positioned above a test window.

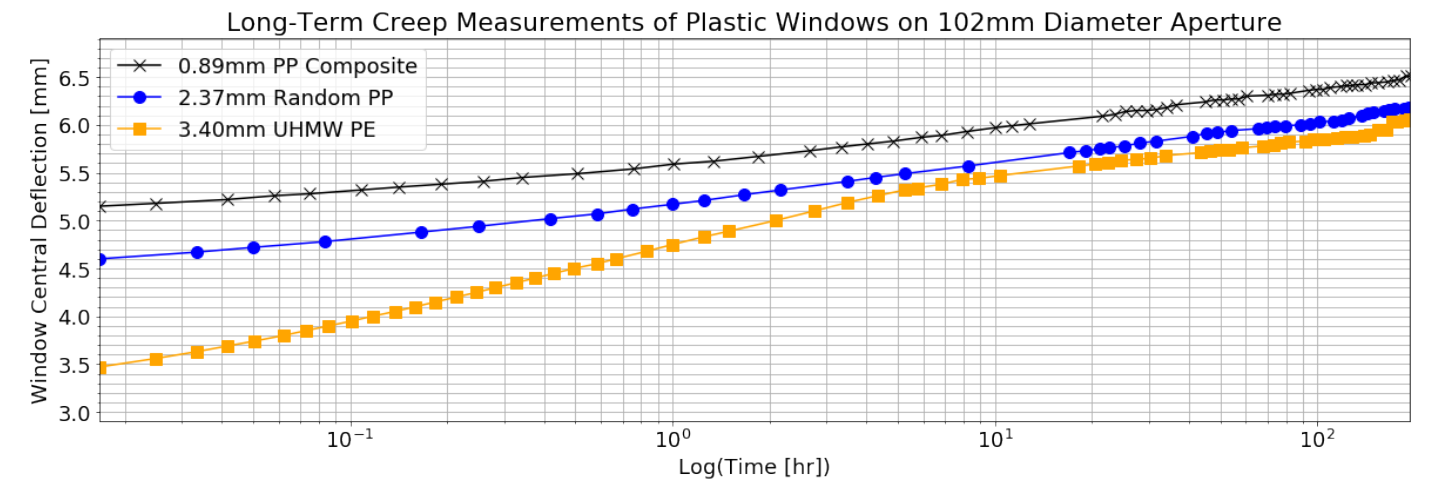

Figure 4: Window Central Deflection vs. Log(Time).

sensitive method, we were able to measure thinner samples, the thicknesses of which are closer to what we will likely use for a window. Results utilizing this technique are included in Table 1.

Mechanical Testing:

The mechanical properties of selected materials have been investigated using the vacuum chamber design shown in Fig. 3. The design of the chamber, with an open aperture of 102 mm in diameter, is based on off-the-shelf vacuum fittings and flanges. The vacuum window sample under test is placed on top of the open flange of an ISO NW-100 tee, on which an O-ring is installed. The sample is pressed against the flange by a metal ring using double claw clamps. The sidearm of the tee is connected to a pressure gauge and a vacuum pump with a shut valve. As the chamber is pumped down, the window material under test is deflected inwards as a result of the pressure differential. This deformation is measured using an electronic drop indicator, positioned near the center of the window. The measured deflection and its rate of change provide an indication of the strength of the material. The phenomenon of creep, which can be pronounced in plastic material, tends to increase the window deflection with time, and the additional strain associated with creep can lead to material failure. For this reason, we have performed long-

Material	Thickness (mm)	Initial Deflection (mm)	Deflection After 300 hours (mm)	Inferred Tensile Modulus (GPa)
Composite PP	0.89	4.9	6.6	2.1
Random PP	2.37	5.1	6.3	0.7
UHMW PE	3.40	4.6	6.1	0.6

Table 2: Central Window Deflection Experimental Results.

term creep monitoring (D. Barkats et al., 2018) which allows us to predict how the deflection will progress over time. Leak-rate measurements can be done by shutting the vacuum valve and monitoring the changing internal pressure. Fig. 4 shows the results of long-term creep measurements conducted in the lab for Composite Polypropylene, Random Polypropylene, and Ultra-High Molecular Weight Polyethylene. The initial deflection is derived from repeated pump-downs. The results from the mechanical testing of some window materials are compiled in Table 2.

Conclusion:

Ultra-High Molecular Weight Polyethylene, Random Polypropylene, and Composite Polypropylene are currently the top candidate materials for the wSMA window due to their combination of mechanical strength and transmission. Once a material is selected, the design of a wide band anti-reflection (AR) coating will commence. Although the progress of this work has been delayed by the recent shutdown of the SMA, we believe that a final choice will be made in the next few months as more data is gathered.

REFERENCES

- C. A. Balanis, Advanced Engineering Electromagnetics. Hoboken, NJ, USA: Wiley, 1989.
- D. Bourreau, A. Peden, and S. Le Maguer, "A quasi-optical free-space measurement setup without time-domain gating for material characterization in the W-Band," IEEE Trans. Instrumentation and Measurement, vol. 55, pp. 2022-2028, 2006.
- C.-Y. E. Tong, A. Hedden, and R. Blundell, "An Empirical Probe to the Operation of SIS Receivers — Revisiting the Technique of Intersecting Lines," 19th IEEE International Symposium on Space THz Technology (ISSTT 2008), Groningen, Netherlands, April 28-30, 2008.
- D. Barkats et al., "Ultra-thin large-aperture vacuum windows for millimeter wavelengths receivers", Proc. SPIE 10708, Millimeter, Submillimeter, and Far-Infrared Detectors and Instrumentation for Astronomy IX, 107082K, July, 2018

RTDC UPDATE

The Radio Telescope Data Center (RTDC) archives and makes available data from the Submillimeter Array (SMA) and other CfA supported telescopes. Listed below are a few significant updates.

- Users will now find it easier to access new data through the SMAOC. PIs and other authorized users will find a download button next to each data file listed in the observing report. This link will take users directly to the pre-selected file in the proprietary archive. Directing users to the archive, rather than initiating a direct download, allows the option of requesting rebinned data.

- The proprietary archive now displays more comprehensive information on the contents of each observation. Results include source names, coordinates, LO tuning, integration time and the number of baselines; this more closely mirrors the public archive format.

- As file sizes increase with the addition of two more SWARM quadrants, it has become imperative to streamline the transfer of data from the summit of Maunakea to the RTDC computers in Cambridge. To meet this requirement we have set up a private network between these sites and put in place a program at the RTDC that regularly scans the summit disks for new (and complete) data directories. If one is identified a transfer is automatically triggered. Once the transfer to Cambridge is complete, it is ingested into the RTDC database and becomes available to request through the proprietary archive. This new software infrastructure will significantly reduce the wait time PIs have experienced before accessing their data.

Website: www.cfa.harvard.edu/rtdc

RECEIVER LAB TALKS

SMA welcomes you to join the 'Receiver Lab Talks' scheduled every Wednesday 1:00 PM EDT (5:00 PM UTC) via Zoom.

Since the lockdown the Receiver Lab has moved their Tuesday 'Lunch Talk' to an online format via Zoom. The talk series has been transformed from a small scale lunch table discussion to an online presentation with a wider range of topics. The focus of the talks are on instrumentation development but they have included subjects ranging from the basics of the SIS mixers, the effect of the atmosphere on submillimeter radiation and future space missions. This talk series has turned out to become a forum to stimulate further development in instrumentation with international contributors throughout the world.

For a list of upcoming and past speakers please view the 'Receiver Lab Talks' webpage:

https://www.cfa.harvard.edu/sma/Projects/LabTalks/

To join the discussion please contact Edward Tong **(etong@cfa.harvard.edu)**

CALL FOR STANDARD OBSERVING PROPOSALS - 2020B SEMESTER

We wish to draw your attention to the latest Call for Standard Observing Proposals for observations with the Submillimeter Array (SMA). This call is for the 2020B semester with observing period **16 Nov 2020 – 15 May 2021.**

Standard Observing Proposals

Submission deadline: **10 September 2020 (US)/11 September 2020 (Taiwan)**

Proposal Information and Submission **http://sma1.sma.hawaii.edu/proposing.html**

The SMA is a reconfigurable interferometric array of eight 6-m antennas on Maunakea jointly built and operated by the Smithsonian Astrophysical Observatory and the Academia Sinica Institute of Astronomy and Astrophysics. The array operates in the 230, 345 and 400 GHz bands, observing simultaneously with two orthogonally polarized receivers, one in the 230 GHz or 345 GHz band and the other in the 240 GHz or 400 GHz band (with full polarimetric observations available using the 230+240 or 345+400 band combinations).

The SMA configurations include antenna separations ranging between 9m and 508 m. The small antennas allow access to low spatial frequencies (with projected baselines as short as 6-m) in the sub-compact configuration, and at the other extreme, the finest angular resolution with the very extended configuration at 345 GHz is ~ 0.25". The compact and extended configurations complete the range. The characteristics, performance and sky coverage of the SMA are both similar and complementary to those of the stand-alone Atacama Compact Array (ACA) component of ALMA, while providing full access to the northern sky.

The heart of the SMA backend is the SWARM correlator, currently expanding to process 12 GHz bandwidth (IF coverage of 4 to 16 GHz) for each receiver in each sideband, for a total of 48 GHz total covered bandwidth, at a uniform 140 kHz resolution. Our delayed start to semester 2020A has pushed the expansion check out back a bit, but we are right now in the final steps of science validation and are confident in its availability in a matter of weeks.

The SMA can tune the orthogonal receiver combinations independently, resulting in a very flexible frequency coverage capability. For example, observations can be made at 1.3mm and 870 micron simultaneously (with many other configurations possible). One popular configuration allows 12 GHz/sideband/receiver frequency coverage to be interleaved, allowing a 44 GHz continous spectral coverage (with 4 GHz of dual polarization coverage), where the tuning ranges overlap for the two orthogonally polarized receivers. Alternatively, the two receivers can be set with the same LO to cover the same 24 GHz (12 GHz in each sideband) of frequency space in the two orthogonal polarizations, allowing improved spectral line sensitivity. In such a case, full Stokes polarization measurements are also possible at 1.3mm and 870 microns.

The SMA provides flexible, wide band frequency coverage that delivers high continuum sensitivity and excellent spectral line capabilities. A full transit observation with the 12 GHz/sideband/receiver correlator coverage will offer continuum sensitivity down to 200 or 450 micro-Jy (1 sigma) at 230 or 345 GHz in good weather conditions (precipitable water vapor 2.5mm and 1.0mm, respectively). The corresponding line sensitivities at 1 km/s resolution are 35 and 80 mJy.

For more information about SMA capabilities, visit the **SMA Observer Center website (http://sma1.sma.hawaii.edu/status.html)** and explore the set of **SMA proposing tools (http://sma1.sma.hawaii.edu/tools.html).** Current and archived **SMA Newsletters (https://www.cfa.harvard.edu/sma/Newsletters/)** provide a sampling of the wide variety of science possible with the SMA.

For more details visit the SMA Observer Center Proposal Information Page at **http://sma1.sma.hawaii.edu/proposing.html**

IMPORTANT DATES FOR STANDARD OBSERVING PROPOSALS
Submissions open: **13 August 2020 (on or before)**
Submissions expected to close: **10 September 2020 (US)/11 September 2020 (Taiwan)**

Given the direct impact of nearly 3 months offline in response to the novel coronavirus pandemic and its potential for continued impact on array operations, current and expected investment in further upgrades to the SMA capabilities, and obligations to previous approved programs, the Large Scale Projects program (for projects requesting 100 to 1000 hours) will not be accepting proposals at this time.

Questions or comments regarding the Standard Observing Proposals can be addressed to **sma-propose@cfa.harvard.edu**.

Mark Gurwell
Chair, Submillimeter Array Time Allocation Committee

POSTDOCTORAL OPPORTUNITIES WITH THE SMA

Applications for the 2021 Submillimeter Array (SMA) Postdoctoral Fellowship program will be due in fall 2020. We anticipate offering one or more SMA Postdoctoral Fellowships starting Summer/Fall 2021.

The SMA is a pioneering radio interferometer designed for arc-second imaging in the submillimeter spectrum. SMA science spans an impressive array of fields, ranging from our solar system, through imaging of gas and dust and tracing magnetic fields in stellar nurseries and planet-forming disks, to exploration of nearby galaxies and imaging of dusty star-forming galaxies at high redshifts. In addition to its outstanding record in astronomical research, the SMA is a world leader in the design of wide-bandwidth, high-frequency radio receivers for astronomy. The SMA commissioned a next generation correlator which vastly increases total bandwidth (to 12 GHz/sideband per polarization per receiver) while retaining high spectral resolution (140 kHz) across the entire processed spectral range, providing significantly enhanced science capability.

These positions are aimed chiefly at research, both observational and theoretical, in submillimeter astronomy as well as instrument development. Successful candidates will participate in remote and on-site observations with the SMA. While the SMA fellowships are intended primarily for research and development associated with the SMA, our main offices at the Center for Astrophysics provide Fellows with unique opportunities to develop collaborations within the broader CfA community of 250 Ph.D. staff researchers and with extraordinary freedom in structuring their research activities. Applicants must have a recent Ph.D. in astronomy or in a related field.

The SMA is a collaboration between the Smithsonian Astrophysical Observatory and the Academia Sinica Institute of Astronomy and Astrophysics in Taipei, Taiwan. The Smithsonian Astrophysical Observatory is an Equal Opportunity/Affirmative

Action Employer where all qualified applicants receive equal consideration without regard to race, color, creed, national origin or gender.

Application information and instructions can be found at:

http://www.cfa.harvard.edu/opportunities/fellowships/sma

The deadline for applications has not yet been determined but is expected to be in no later than October 2020. Please check the above link for up to date information on the deadline and application procedure.

Questions: **smapostdoc@cfa.harvard.edu**

SMA POSTDOCTORAL FELLOWS: COMINGS AND GOINGS

The Submillimeter Array Postdoctoral Fellowship program supports early career scientists active in a variety of astronomical research fields involving submillimeter astronomy. The SMA Fellowship is competitive, and a high percentage of our past Fellows have gone on to permanent faculty and research staff positions located around the world.

The SMA welcomes our newest Fellows:

Kirsten Hall is finishing her Ph.D. work at Johns Hopkins University, with the thesis 'Understanding Galaxy Evolution with Far-infrared and Millimeter Datasets' (advisor: Nadia Zakamska). Kirsten's research is focused on galaxy evolution and large scale structures. She will join the Center for Astrophysics in 2020 as a Schmidt Science Fellow and is expected to take up the SMA fellowship in 2021.

Eric W. Koch is finishing his Ph.D. work at University of Alberta, Canada, with the thesis 'The Molecular and Atomic Interstellar Medium in the Local Group' (adviser: Erik Rosolowsky). Eric's research is in observational astronomy related to interstellar medium in galaxies, with particular interests in studying the atomic and molecular gas in M33. He also contributes to developing analysis tools for common use in astronomy.

Wei Yu received his Ph.D. from TongJi University, China in 2020, with the thesis 'Research on Encoding and Decoding Methods of Analog Chaotic Codes and Raptor Codes Based on Information Theory' (advisor: Jun Wu). Wei's expertise is in computer science, with particular interests in developing radio astronomy instrumentation and software.

Hall, Koch and Yu will take up their fellowship in fall 2020. They join continuing SMA Fellows **Andrew Burkhardt, John Garrett, Feng Long** and **Richard Teague**.

As new Fellows arrive, we also take the time to thank those Fellows who have moved on to even bigger things:

Luca Matrà moved to Galway, Ireland recently to take up a faculty position as Lecturer in Astronomy at the National University of Ireland Galway (NUIG). There, he will continue his research on exocometary belts around nearby stars as part of a new (sub) millimeter astronomy group.

Maria Jesus Jiménez-Donaire has moved to Spain to become a staff astronomer at the National Astronomy Observatory in Madrid (OAN-IGN), a part of the National Geographic Institute at the Ministry of Development. She joined the groups of galactic and extra galactic star formation at the Observatory, and will continue to pursue her research on star formation in galaxies while working on improving the 40m Telescope at the Yebes Observatory.

We wish all our current and former Fellowship holders continued success!

A list of current and former SMA Fellows is provided at **https://www.cfa.harvard.edu/opportunities/fellowships/sma/smafellows.html** along with further information on the SMA Fellowship program. We anticipate the deadline for the 2021 SMA Fellowship opportunities will be in October 2020.

Qizhou Zhang
Chair, SMA Fellowship Selection Committee

STAFF CHANGES IN HILO

Ramprasad Rao, Physicist, joined SAO in February, reporting to Simon Radford. Ram earned his PhD in astronomy at the University of Illinois, held postdoctoral appointments at the University of Chicago and at SAO, and has been a research astronomer on the ASIAA staff supporting the SMA in Hilo. He will oversee science observations, including scheduling projects, evaluating data quality, and supervising the telescope operators.

Travis Nelson, Astrophysicist (Telescope Operator), joined SAO in March, reporting to Ram Rao. He recently earned his PhD in physics at the University of Hawai'i.

Jennie Berghuis, Astrophysicist (Telescope Operator), left the SMA in March to take a position at the Gemini Observatory. We thank Jennie for her efforts and wish her success in the future.

Brian Force, Electronics Technician, left the SMA in July to take a position at the US Merchant Marine Academy. Over the past three decades, Brian worked at, and contributed to, four of the Maunakea observatories: CSO, JCMT, Keck, and the SMA. During almost six years at the SMA, Brian was primarily responsible for the correlators, initially maintenance of the ASIC correlator until its decommissioning in 2016 and then installation and upkeep of the present SWARM correlator. He also devoted considerable effort to developing electronics for the upcoming wSMA receivers. We thank Brian for his efforts and wish him success in the future.

PROPOSAL STATISTICS 2020A (16 MAY 2020 – 15 NOV 2020)

The SMA received a total of 66 proposals (SAO 59) requesting observing time in the 2020A semester. The proposals received by the joint SAO and ASIAA Time Allocation Committee are divided among science categories as follows:

CATEGORY	PROPOSALS
high mass (OB) star formation, cores	17
local galaxies, starbursts, AGN	11
low/intermediate mass star formation, cores	10
submm/hi-z galaxies	10
protoplanetary, transition, debris disks	7
GRB, SN, high energy	4
evolved stars, AGB, PPN	2
solar system	2
Galactic center	1
UH	1
other	1

TRACK ALLOCATIONS BY WEATHER REQUIREMENT (ALL PARTNERS):

PWV[1]	SAO	ASIAA	UH[2]
< 4.0mm	23A + 42B	5A + 4B	0
< 2.5mm	25A + 27B	6A + 1B	4
< 1.0mm	1A + 0B	0A + 0B	0
Total	**49A + 69B**	**11A + 5B**	**4**

(1) Precipitable water vapor required for the observations.

(2) UH does not list As and Bs.

TOP-RANKED 2020A SEMESTER PROPOSALS

The following is the listing of all SAO and ASIAA proposals with at least a partial A ranking with the names and affiliations of the principal investigators.

GRB, SN, HIGH ENERGY

Anna Ho, Caltech
A new class of energetic stellar explosions in a dense medium

Kuiyun Huang, CYCU
Multi-frequency follow-ups of Short GRBs

HIGH MASS (OB) STAR FORMATION, CORES

Henrik Beuther, MPIfR
The importance of magnetic fields for the fragmentation of high-mass star-forming regions (the remaining summer targets)

Jia-Wei Wang, ASIAA
Resolve the polarization morphology from the envelope to the Keplerian disk at 200 AU scale in the massive protostar Cepheus A HW2

Qizhou Zhang, CfA
Magnetic Fields and protocluster formation

Todd Hunter, NRAO
Triggered follow-up of accretion outbursts in massive protostars

LOCAL GALAXIES, STARBURSTS, AGN

Glen Petitpas, CfA
The Beautiful and Enigmatic Spiral Galaxy NGC 7331

LOW/INTERMEDIATE MASS STAR FORMATION, CORES

Manar el Akel, Observatory of Paris, LERMA
The Rosetta stone to sulfur: H2S from laboratory to observations

PROTOPLANETARY, TRANSITION, DEBRIS DISKS

Hau-Yu Baobab Liu, ASIAA
Millimeter Flux Variability/Stability of FU Orionis Objects and EXors

Richard Teague, CfA
A 3D Exploration of an Edge-On Self-Gravitating Disk

Romane Le Gal, CfA
Sulfur Chemistry in Planet-forming Disks

SOLAR SYSTEM

Charlie Qi, CfA
Imaging of Comet C/2019 Y4(ATLAS)

Mark Gurwell, CfA
Polarized Emission from the Surface of Mars

SUBMM/HI-Z GALAXIES

Chian-Chou Chen, ASIAA
Pinpointing the dusty star-forming galaxies around the Slug ELAN

Jaclyn Champagne, University of Texas at Austin
Searching for the Cores of the Most Massive Galaxy Protoclusters at 2

Kirsten Hall, Johns Hopkins University
Constraining dust spectra and detecting hot quasar winds via the thermal Sunyaev-Zel'dovich Effect

Rohit Kondapally, University of Edinburgh
Revealing the nature of the most extreme, dusty, LOFAR-identified galaxies at 3

OTHER

Romane Le Gal, CfA
First unbiased interferometric molecular survey of PDRs: NGC 7023 NW and 2023 S

SAO PROPOSALS 2019B SEMESTER

The following is the listing of all SAO proposals at least partially observed in the 2019B semester (16 Nov 2019 – 15 May 2020).

Matthew Ashby, CfA
An Exploration of Nitrogen Gas Content in Protoplanetary Disks (2018B-S046 Continuation)

Dana Anderson, Caltech
The Impact of Radio Jets on Star Formation in AGN Host Galaxies, Part II

Andrew Burkhardt, CfA
AY191 Spring 2020 SMA Project

Joseph Cairns, Imperial College London
Cluster Cores at z > 4

Gianluca Castignani, École Polytechnique Fédérale de Lausanne
Environment effect in cosmic filaments: mapping CO in HI-deficient galaxies

Yang Chen, Nanjing University
Search for multi-chemical lines with the SMA

Lennox Cowie, University of Hawaii
SMA identification of submm sources behind 3 northern clusters

Somnath Dutta, ASIAA
Mapping B-field structure in the envelope of the protostellar system HH 111

Naomi Hirano, ASIAA
Magnetic fields in the central regions of prestellar cores

Anna Ho, Caltech
The death throes of massive stars, revealed through early millimeter observations

Garrett Keating, CfA
2020 Submillimeter Array Interferometry School Projects

Garrett Keating, CfA
Untangling the Molecular Mystery of An Unusual High-Redshift Galaxy

Chia-Lin Ko, National Tsing Hua University
Abundance ratios of S-bearing molecules as an alternative probe of grain growth

Attila Kovacs, CfA
Active Sunyaev-Zel'dovich clusters: sub-structure and starburst galaxies within

Romane Le Gal, CfA
First unbiased interferometric molecular survey of PDRs: NGC 7023 NW and 2023 S

Hau-Yu Baobab Liu, ASIAA
Millimeter Flux Variability/Stability of FU Orionis Objects and EXors

Feng Long, CfA
Long The Synergy between SMA and ALMA: test disk formation and evolution models

Goran Sandell, University of Hawaii
NGC 2261 molecular outflow

Jamila Pegues, CfA
SMA Survey of Chemistry in Herbig Ae/Be Protoplanetary Disks

Giulia Perotti, University of Copenhagen
Mind the gap: linking ice and gas around R CrA

Evan Rich, University of Michigan
Gmeini-LIGHTS Survey: Flux and Gas Dynamics of Never Before Observed Protoplanetary Disks

Andra Stroe, CfA
A Complete Census of the Molecular Gas Reservoirs in the Antlia Cluster

Jia-Wei Wang, ASIAA
Probe the multi-scale magnetic fields within the intermediate mass hub-filament system OMC2-FIR4

Jonathan Williams, University of Hawaii
The kilo-au environments of T Tauri stars

Ya-Lin Wu, University of Texas, Austin
Probing the Giant Molecular Clouds in NGC 5055

RECENT PUBLICATIONS

TITLE: CMZoom: Survey Overview and First Data Release
AUTHORS: Battersby, Cara; Keto, Eric; Walker, Daniel; Barnes, Ashley; Callanan, Daniel; Ginsburg, Adam; Hatchfield, H Perry; Henshaw, Jonathan; Kauffmann, Jens; Kruijssen, J. M. Diederik; Longmore, Steven N.; Lu, Xing; Mills, Elisabeth A. C.; Pillai, Thushara; Zhang, Qizhou; Bally, John; Butterfield, Natalie; Contreras, Yanett A.; Ho, Luis C.; Ott, Jurgen Patel, Nimesh; Tolls, Volker
PUBLICATION: *eprint arXiv:2007.05023*
PUB DATE: July 2020
ABSTRACT: https://ui.adsabs.harvard.edu/abs/2020arXiv200705023B/abstract

---

TITLE: Multiwavelength Analysis of the Variability of the Blazar 3C 273
AUTHORS: Fernandes, Sunil; Patiño-Álvarez, Víctor M.; Chavushyan, Vahram; Schlegel, Eric M.; Ramón Valdés, José
PUBLICATION: *eprint arXiv:2007.03105*
PUB DATE: July 2020
ABSTRACT: https://ui.adsabs.harvard.edu/abs/2020arXiv200703105F/abstract

---

TITLE: Multi-wavelength, spatially resolved modelling of HD 48682's debris disc
AUTHORS: Hengst, S.; Marshall, J. P.; Horner, J.; Marsden, S. C.
PUBLICATION: *Monthly Notices of the Royal Astronomical Society, Advance Access*
PUB DATE: July 2020
ABSTRACT: https://ui.adsabs.harvard.edu/abs/2020MNRAS.tmp.2092H/abstract

---

TITLE: Molecular remnant of Nova 1670 (CK Vulpeculae): Properties and enigmatic origin of the gas
AUTHOR: Kaminski, T.; Menten, K. M.; Tylenda, R.; Wong, K. T.; Belloche, A.; Mehner, A.; Schmidt, M. R.; Patel, N. A.
PUBLICATION: *eprint arXiv:2006.10471*
PUB DATE: June 2020
ABSTRACT: https://ui.adsabs.harvard.edu/abs/2020arXiv200610471K/abstract

---

TITLE: The Nature of 500 micron Risers I: SMA Observations
AUTHOR: Greenslade, J.; Clements, D. L.; Petitpas, G.; Asboth, V.; Conley, A.; Pérez-Fournon, I.; Riechers, D.
PUBLICATION: *Monthly Notices of the Royal Astronomical Society, Advance Access*
PUB DATE: June 2020
ABSTRACT: https://ui.adsabs.harvard.edu/abs/2020MNRAS.tmp.1793G/abstract

---

TITLE: SN2020bvc: a Broad-lined Type Ic Supernova with a Double-peaked Optical Light Curve and a Luminous X-ray and Radio Counterpart

AUTHOR: Ho, A. Y. Q.; Kulkarni, S. R.; Perley, D. A.; Cenko, S. B.; Corsi, A.; Schulze, S.; Lunnan, R.; Sollerman, J.; Gal-Yam, A.; Anand, S.; Barbarino, C.; Bellm, E.; Bruch, R.; Burns, E.; De, K.; Dekany, R.; Delacroix, A.; Duev, D.; Fremling, C.; Goldstein, D. Golkhou, Z.; Graham, M. J.; Hale, D.; Kasliwal, M. M.; Kupfer, T.; Laher, R.; Martikainen, J.; Masci, F. J.; Neill, J. D.; Rusholme, B.; Shupe, D. L.; Soumagnac, M. T.; Strotjohann, N. L.; Taggart, K.; Tartaglia, L.; Yan, L.; Zolkower, J.

PUBLICATION: *eprint arXiv:2004.10406*

PUB DATE: April 2020

ABSTRACT: https://ui.adsabs.harvard.edu/abs/2020arXiv200410406H/abstract

---

TITLE: SYMBA: An end-to-end VLBI synthetic data generation pipeline. Simulating Event Horizon Telescope observations of M 87

AUTHOR: Roelofs, F.; Janssen, M.; Natarajan, I.; Deane, R.; Davelaar, J.; Olivares, H.; Porth, O.; Paine, S. N.; Bouman, K. L.; Tilanus, R. P. J.; van Bemmel, I. M.; Falcke, H.; Akiyama, K.; Alberdi, A.; Alef, W.; Asada, K.; Azulay, R.; Baczko, A.; Ball, D.; Baloković, M. Barrett, J.; Bintley, D.; Blackburn, L.; Boland, W.; Bower, G. C.; Bremer, M.; Brinkerink, C. D.; Brissenden, R.; Britzen, S.; Broderick, A. E.; Broguiere, D.; Bronzwaer, T.; Byun, D.; Carlstrom, J. E.; Chael, A.; Chan, C.; Chatterjee, S.; Chatterjee, K.; Chen, M.; Chen, Y.; Cho, I.; Christian, P.; Conway, J. E.; Cordes, J. M.; Crew, G. B.; Cui, Y.; De Laurentis, M.; Dempsey, J.; Desvignes, G.; Dexter, J.; Doeleman, S. S.; Eatough, R. P.; Fish, V. L.; Fomalont, E.; Fraga-Encinas, R.; Friberg, P.; Fromm, C. M.; Gómez, J. L.; Galison, P.; Gammie, C. F.; García, R.; Gentaz, O.; Georgiev, B.; Goddi, C.; Gold, R.; Gu, M.; Gurwell, M.; Hada, K.; Hecht, M. H.; Hesper, R.; Ho, L. C.; Ho, P.; Honma, M.; Huang, C. L.; Huang, L.; Hughes, D. H.; Ikeda, S.; Inoue, M.; Issaoun, S.; James, D. J.; Jannuzi, B. T.; Jeter, B.; Jiang, W.; Johnson, M. D.; Jorstad, S.; Jung, T.; Karami, M.; Karuppusamy, R.; Kawashima, T.; Keating, G. K.; Kettenis, M.; Kim, J.; Kim, J.; Kim, J.; Kino, M.; Koay, J. Y.; Koch, P. M.; Koyama, S.; Kramer, M.; Kramer, C.; Krichbaum, T. P.; Kuo, C.; Lauer, T. R.; Lee, S.; Li, Y.; Li, Z.; Lindqvist, M.; Lico, R.; Liu, K.; Liuzzo, E.; Lo, W.; Lobanov, A. P.; Loinard, L.; Lonsdale, C.; Lu, R.; MacDonald, N. R.; Mao, J.; Markoff, S.; Marrone, D. P.; Marscher, A. P.; Martí-Vidal, I.; Matsushita, S.; Matthews, L. D.; Medeiros, L.; Menten, K. M.; Mizuno, Y.; Mizuno, I.; Moran, J. M.; Moriyama, K.; Moscibrodzka, M.; Müller, C.; Nagai, H.; Nagar, N. M.; Nakamura, M.; Narayan, R.; Narayanan, G.; Neri, R.; Ni, C.; Noutsos, A.; Okino, H.; Olivares, H.; Ortiz-León, G. N.; Oyama, T.; Özel, F.; Palumbo, D. C. M.; Patel, N.; Pen, U.; Pesce, D. W.; Piétu, V.; Plambeck, R.; PopStefanija, A.; Prather, B.; Preciado-López, J. A.; Psaltis, D.; Pu, H.; Ramakrishnan, V.; Rao, R.; Rawlings, M. G.; Raymond, A. W.; Rezzolla, L.; Ripperda, B.; Rogers, A.; Ros, E.; Rose, M.; Roshanineshat, A.; Rottmann, H.; Roy, A. L.; Ruszczyk, C.; Ryan, B. R.; Rygl, K. L. J.; Sánchez, S.; Sánchez-Arguelles, D.; Sasada, M.; Savolainen, T.; Schloerb, F. P.; Schuster, K.; Shao, L.; Shen, Z.; Small, D.; Won Sohn, B.; SooHoo, J.; Tazaki, F.; Tiede, P.; Titus, M.; Toma, K.; Torne, P.; Traianou, E.; Trent, T.; Trippe, S.; Tsuda, S.; van Langevelde, H. J.; van Rossum, D. R.; Wagner, J.; Wardle, J.; Weintroub, J.; Wex, N.; Wharton, R.; Wielgus, M.; Wong, G. N.; Wu, Q.; Young, A.; Young, K.; Younsi, Z.; Yuan, F.; Yuan, Y.; Zensus, J. A.; Zhao, G.; Zhao, S.; Zhu, Z.

PUBLICATION: *Astronomy & Astrophysics, Volume 636, id.A5, 19 pp.*

PUB DATE: April 2020

ABSTRACT: https://ui.adsabs.harvard.edu/abs/2020A%26A...636A...5R/abstract

---

TITLE: Physical Conditions and Kinematics of the Filamentary Structure in Orion Molecular Cloud 1

AUTHOR: Teng, Yu-Hsuan; Hirano, Naomi

PUBLICATION: *The Astrophysical Journal, Volume 893, Issue 1, id.63*

PUBLICATION DATE: April 2020

ABSTRACT: https://ui.adsabs.harvard.edu/abs/2020ApJ...893...63T/abstract

---

TITLE: A three-dimensional view of Gomez's hamburger

AUTHOR: Teague, Richard; Jankovic, Marija R.; Haworth, Thomas J.; Qi, Chunhua; Ilee, John D.

PUBLICATION: *Monthly Notices of the Royal Astronomical Society, Volume 495, Issue 1, pp.451-459*

PUBLICATION DATE: April 2020

ABSTRACT: https://ui.adsabs.harvard.edu/abs/2020MNRAS.495..451T/abstract

---

TITLE: Two-component Jets of GRB 160623A as Shocked Jet Cocoon Afterglow
AUTHOR: Chen, Wei Ju; Urata, Yuji; Huang, Kuiyun; Takahashi, Satoko; Petitpas, Glen; Asada, Keiichi
PUBLICATION: *The Astrophysical Journal Letters, Volume 891, Issue 1, id.L15*
PUBLICATION DATE: March 2020
ABSTRACT: https://ui.adsabs.harvard.edu/abs/2020ApJ...891L..15C/abstract

---

TITLE: Rapid grain growth in post-AGB disc systems from far-infrared and sub-millimetre photometry
AUTHOR: Scicluna, P.; Kemper, F.; Trejo, A.; Marshall, J. P.; Ertel, S.; Hillen, M.
PUBLICATION: *Monthly Notices of the Royal Astronomical Society, Volume 494, Issue 2, pp.2925-2936*
PUBLICATION DATE: February 2020
ABSTRACT: https://ui.adsabs.harvard.edu/abs/2020MNRAS.494.2925S/abstract

---

TITLE: Flare-like Variability of the Mg II λ2798 Å Emission Line and UV Fe II Band in the Blazar CTA 102
AUTHOR: Chavushyan, Vahram; Patiño-Álvarez, Victor M.; Amaya-Almazán, Raúl A.; Carrasco, Luis
PUBLICATION: *The Astrophysical Journal, Volume 891, Issue 1, id.68*
PUBLICATION DATE: March 2020
ABSTRACT: https://ui.adsabs.harvard.edu/abs/2020ApJ...891...68C/abstract

---

TITLE: Multiwavelength behaviour of the blazar 3C 279: decade-long study from γ-ray to radio
AUTHOR: Larionov, V. M.; Jorstad, S. G.; Marscher, A. P.; Villata, M.; Raiteri, C. M.; Smith, P. S.; Agudo, I.; Savchenko, S. S.; Morozova, D. A.; Acosta-Pulido, J. A.; Aller, M. F.; Aller, H. D.; Andreeva, T. S.; Arkharov, A. A.; Bachev, R.; Bonnoli, G.; Borman, G. A.; Bozhilov, V.; Calcidese, P.; Carnerero, M. I. Carosati, D.; Casadio, C.; Chen, W. -P.; Damljanovic, G.; Dementyev, A. V.; Di Paola, A.; Frasca, A.; Fuentes, A.; Gómez, J. L.; Gónzalez-Morales, P.; Giunta, A.; Grishina, T. S.; Gurwell, M. A.; Hagen-Thorn, V. A.; Hovatta, T.; Ibryamov, S.; Joshi, M.; Kiehlmann, S.; Kim, J. -Y.; Kimeridze, G. N.; Kopatskaya, E. N.; Kovalev, Yu A.; Kovalev, Y. Y.; Kurtanidze, O. M.; Kurtanidze, S. O.; Lähteenmäki, A.; Lázaro, C.; Larionova, L. V.; Larionova, E. G.; Leto, G.; Marchini, A.; Matsumoto, K.; Mihov, B.; Minev, M.; Mingaliev, M. G.; Mirzaqulov, D.; Muñoz Dimitrova, R. V.; Myserlis, I.; Nikiforova, A. A.; Nikolashvili, M. G.; Nizhelsky, N. A.; Ovcharov, E.; Pressburger, L. D.; Rakhimov, I. A.; Righini, S.; Rizzi, N.; Sadakane, K.; Sadun, A. C.; Samal, M. R.; Sanchez, R. Z.; Semkov, E.; Sergeev, S. G.; Sigua, L. A.; Slavcheva-Mihova, L.; Sola, P.; Sotnikova, Yu V.; Strigachev, A.; Thum, C.; Traianou, E.; Troitskaya, Yu V.; Troitsky, I. S.; Tsybulev, P. G.; Vasilyev, A. A.; Vince, O.; Weaver, Z. R.; Williamson, K. E.; Zhekanis, G. V.
PUBLICATION: *Monthly Notices of the Royal Astronomical Society, Volume 492, Issue 3, p.3829-3848*
PUBLICATION DATE: March 2020
ABSTRACT: https://ui.adsabs.harvard.edu/abs/2020MNRAS.492.3829L/abstract

---

TITLE: Broadband Variability and Correlation Study of 3C 279 during Flares of 2017–2018
AUTHOR: Prince, Raj
PUBLICATION: *The Astrophysical Journal, Volume 890, Issue 2, id.164*
PUBLICATION DATE: February 2020
ABSTRACT: https://ui.adsabs.harvard.edu/abs/2020ApJ...890..164P/abstract

---

TITLE: First Resolved Dust Continuum Measurements of Individual Giant Molecular Clouds in the Andromeda Galaxy
AUTHOR: Forbrich, Jan; Lada, Charles J.; Viaene, Sébastien; Petitpas, Glen
PUBLICATION: *The Astrophysical Journal, Volume 890, Issue 1, id.42*
PUBLICATION DATE: February 2020
ABSTRACT: https://ui.adsabs.harvard.edu/abs/2020ApJ...890...42F/abstract

---

TITLE: SOFIA/HAWC+ View of an Extremely Luminous Infrared Galaxy: WISE 1013+6112
AUTHOR: Toba, Yoshiki; Wang, Wei-Hao; Nagao, Tohru; Ueda, Yoshihiro; Ueda, Junko; Lim, Chen-Fatt; Chang, Yu-Yen; Saito, Toshiki; Kawabe, Ryohei
PUBLICATION: *The Astrophysical Journal, Volume 889, Issue 2, id.76*
PUBLICATION DATE: February 2020
ABSTRACT: https://ui.adsabs.harvard.edu/abs/2020ApJ...889...76T/abstract

---

TITLE: Localizing the γ-ray emitting region in the blazar TXS 2013+370
AUTHOR: Traianou, E.; Krichbaum, T. P.; Boccardi, B.; Angioni, R.; Rani, B.; Liu, J.; Ros, E.; Bach, U.; Sokolovsky, K. V.; Lisakov, M. M.; Kiehlmann, S.; Gurwell, M.; Zensus, J. A.
PUBLICATION: *Astronomy & Astrophysics, Volume 634, id.A112, 16 pp.*
PUBLICATION DATE: February 2020
ABSTRACT: https://ui.adsabs.harvard.edu/abs/2020A%26A...634A.112T/abstract

---

TITLE: A SCUBA-2 selected Herschel-SPIRE dropout and the nature of this population
AUTHOR: Greenslade, J.; Aguilar, E.; Clements, D. L.; Dannerbauer, H.; Cheng, T.; Petitpas, G.; Yang, C.; Messias, H.; Oteo, I.; Farrah, D.; Michałowski, M. J.; Pérez Fournon, I.; Aretxaga, I.; Yun, M. S.; Eales, S.; Dunne, L.; Cooray, A.; Andreani, P.; Hughes, D. H.; Velázquez, M. Sánchez-Argüelles, D.; Ponthieu, N.
PUBLICATION: *Monthly Notices of the Royal Astronomical Society, Volume 490, Issue 4, p.5317-5334*
PUBLICATION DATE: December 2019
ABSTRACT: https://ui.adsabs.harvard.edu/abs/2019MNRAS.490.5317G/abstract

---

TITLE: The Interaction between the Supernova Remnant W41 and the Filamentary Infrared Dark Cloud G23.33-0.30
AUTHOR: Hogge, Taylor G.; Jackson, James M.; Allingham, David; Guzman, Andres E.; Killerby-Smith, Nicholas; Kraemer, Kathleen E.; Sanhueza, Patricio; Stephens, Ian W.; Whitaker, J. Scott
PUBLICATION: *The Astrophysical Journal, Volume 887, Issue 1, article id. 79, 17 pp. (2019).*
PUBLICATION DATE: December 2019
ABSTRACT: https://ui.adsabs.harvard.edu/abs/2019ApJ...887...79H/abstract

---

TITLE: Investigating the multiwavelength behaviour of the flat spectrum radio quasar CTA 102 during 2013-2017
AUTHOR: D'Ammando, F.; Raiteri, C. M.; Villata, M.; Acosta-Pulido, J. A.; Agudo, I.; Arkharov, A. A.; Bachev, R.; Baida, G. V.; Benítez, E.; Borman, G. A.; Boschin, W.; Bozhilov, V.; Butuzova, M. S.; Calcidese, P.; Carnerero, M. I.; Carosati, D.; Casadio, C.; Castro-Segura, N.; Chen, W. -P.; Damljanovic, G. Di Paola, A.; Echevarría, J.; Efimova, N. V.; Ehgamberdiev, Sh A.; Espinosa, C.; Fuentes, A.; Giunta, A.; Gómez, J. L.; Grishina, T. S.; Gurwell, M. A.; Hiriart, D.; Jermak, H.; Jordan, B.; Jorstad, S. G.; Joshi, M.; Kimeridze, G. N.; Kopatskaya, E. N.; Kuratov, K.; Kurtanidze, O. M.; Kurtanidze, S. O.; Lähteenmäki, A.; Larionov, V. M.; Larionova, E. G.; Larionova, L. V.; Lázaro, C.; Lin, C. S.; Malmrose, M. P.; Marscher, A. P.; Matsumoto, K.; McBreen, B.; Michel, R.; Mihov, B.; Minev, M.; Mirzaqulov, D. O.; Molina, S. N.; Moody, J. W.; Morozova, D. A.; Nazarov, S. V.; Nikiforova, A. A.; Nikolashvili, M. G.; Ohlert, J. M.; Okhmat, N.; Ovcharov, E.; Pinna, F.; Polakis, T. A.; Protasio, C.; Pursimo, T.; Redondo-Lorenzo, F. J.; Rizzi, N.; Rodriguez-Coira, G.; Sadakane, K.; Sadun, A. C.; Samal, M. R.; Savchenko, S. S.; Semkov, E.; Sigua, L.; Skiff, B. A.; Slavcheva-Mihova, L.; Smith, P. S.; Steele, I. A.; Strigachev, A.; Tammi, J.; Thum, C.; Tornikoski, M.; Troitskaya, Yu V.; Troitsky, I. S.; Vasilyev, A. A.; Vince, O.; WEBT Collaboration; Hovatta, T; Kiehlmann, S.; Max-Moerbeck, W.; Readhead, A. C. S.; Reeves, R.; Pearson, T. J.; OVRO Team; Mufakharov, T; Sotnikova, Yu V.; Mingaliev, M. G.
PUBLICATION: *Monthly Notices of the Royal Astronomical Society, Volume 490, Issue 4, p.5300-5316*
PUBLICATION DATE: December 2019
ABSTRACT: https://ui.adsabs.harvard.edu/abs/2019MNRAS.490.5300D/abstract

---

TITLE: Evidence for Late-stage Eruptive Mass Loss in the Progenitor to SN2018gep, a Broad-lined Ic Supernova: Pre-explosion Emission and a Rapidly Rising Luminous Transient

AUTHOR: Ho, Anna Y. Q.; Goldstein, Daniel A.; Schulze, Steve; Khatami, David K.; Perley, Daniel A.; Ergon, Mattias; Gal-Yam, Avishay; Corsi, Alessandra; Andreoni, Igor; Barbarino, Cristina; Bellm, Eric C.; Blagorodnova, Nadia; Bright, Joe S.; Burns, E.; Cenko, S. Bradley; Cunningham, Virginia; De, Kishalay; Dekany, Richard; Dugas, Alison; Fender, Rob P. Fransson, Claes; Fremling, Christoffer; Goldstein, Adam; Graham, Matthew J.; Hale, David; Horesh, Assaf; Hung, Tiara; Kasliwal, Mansi M.; Kuin, N. Paul M.; Kulkarni, S. R.; Kupfer, Thomas; Lunnan, Ragnhild; Masci, Frank J.; Ngeow, Chow-Choong; Nugent, Peter E.; Ofek, Eran O.; Patterson, Maria T.; Petitpas, Glen; Rusholme, Ben; Sai, Hanna; Sfaradi, Itai; Shupe, David L.; Sollerman, Jesper; Soumagnac, Maayane T.; Tachibana, Yutaro; Taddia, Francesco; Walters, Richard; Wang, Xiaofeng; Yao, Yuhan; Zhang, Xinhan

PUBLICATION: *The Astrophysical Journal, Volume 887, Issue 2, article id. 169, 24 pp. (2019).*

PUBLICATION DATE: December 2019

ABSTRACT: https://ui.adsabs.harvard.edu/abs/2019ApJ...887..169H/abstract

The Submillimeter Array (SMA) is a pioneering radio-interferometer dedicated to a broad range of astronomical studies including finding protostellar disks and outflows; evolved stars; the Galactic Center and AGN; normal and luminous galaxies; and the solar system. Located on Maunakea, Hawaii, the SMA is a collaboration between the Smithsonian Astrophysical Observatory and the Academia Sinica Institute of Astronomy and Astrophysics.

SUBMILLIMETER ARRAY
Center for Astrophysics | Harvard & Smithsonian
60 Garden Street, MS 78
Cambridge, MA 02138 USA
www.cfa.harvard.edu/sma/

SMA HILO OFFICE
645 North A'ohoku Place
Hilo, Hawaii 96720
Ph. 808.961.2920
Fx. 808.961.2921
sma1.sma.hawaii.edu

ACADEMIA SINICA INSTITUTE
OF ASTRONOMY & ASTROPHYSICS
11F of Astronomy-Mathematics Building,
AS/NTU, No. 1, Sec. 4, Roosevelt Road
Taipei 10617
Taiwan R.O.C.
www.asiaa.sinica.edu.tw/